Fuel Cell

Byungwoo Park

Department of Materials Science and Engineering
Seoul National University

http://bp.snu.ac.kr

Environment-Friendly Power Sources

Laptop

Samsung SDI

Cellular Phone

LG Chem.

Power Sources for the Next Generation

LEV

Hyundai Motor

PMP

Samsung SDI

Fuel Cell (PEMFC: η = 83% / DMFC: η = 97% at 298 K)

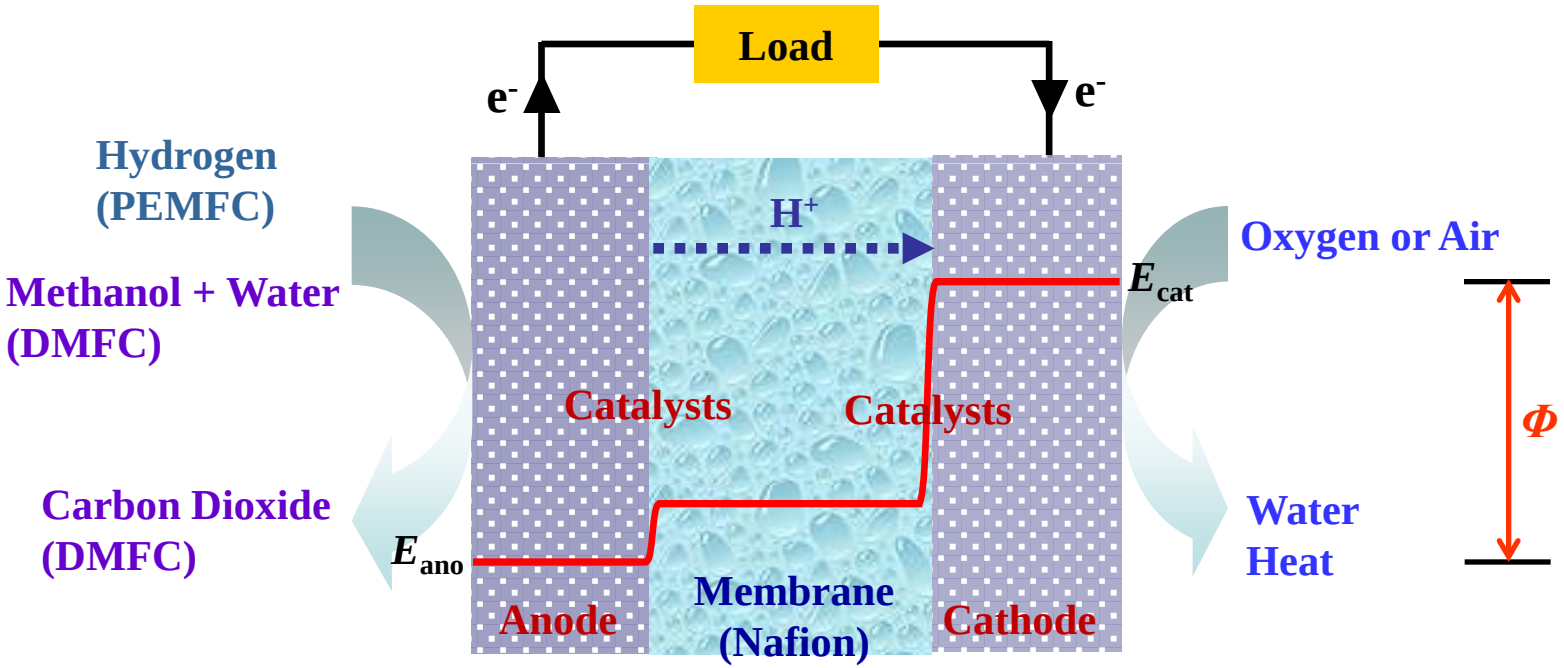

$2H_2 \leftrightarrow 4H^+ + 4e^-$
E_{ano} = 0 V (Hydrogen Oxidation)

$CH_3OH + H_2O \leftrightarrow CO_2 + 6H^+ + 6e^-$
E_{ano} = 0.05 V (Methanol Oxidation)

PEMFC (1.23 V)

DMFC (1.18 V)

$O_2 + 4H^+ + 4e^- \leftrightarrow 2H_2O$
E_{cat} = 1.23 V (Oxygen Reduction)

$3/2\,O_2 + 6H^+ + 6e^- \leftrightarrow 3H_2O$
E_{cat} = 1.23 V (Oxygen Reduction)

- **Goals:**
  - Catalytic Activity
  - Stability

➡ *Nanostructured Materials*

- 2010-11-03

Produced electrical energy

Maximum efficiency possible = (Thermodynamic efficiency)

$$\frac{\Delta G\,(T_1)}{\Delta H\,(T_1)} \times 100\%$$

Total enthalpy produced during a chemical reaction

$\Delta G = \Delta H - T\Delta S$

Thermodynamic Efficiency = 100% at 0 K.

Change in Gibbs free energy

Table 2.2 $\Delta\bar{g}_f$, maximum EMF, and efficiency limit (ref. HHV) for hydrogen fuel cells

Form of water product	Temp °C	$\Delta\bar{g}_f$, kJ/mole	Max EMF	Efficiency limit
Liquid	25	-237.2	1.23V	83%
Liquid	80	-228.2	1.18V	80%
Gas	100	-225.3	1.17V	79%
Gas	200	-220.4	1.14V	77%
Gas	400	-210.3	1.09V	74%
Gas	600	-199.6	1.04V	70%
Gas	800	-188.6	0.98V	66%
Gas	1000	-177.4	0.92V	62%

J. Larminie and A. Dicks
Fuel cell systems Explained, p. 25, (2000).

Change in Enthalpy

$$H_2 + \tfrac{1}{2}O_2 \rightarrow H_2O \quad (steam)$$
$$\Delta\bar{h}_f = -241.83 \; kJ/mole$$
$$H_2 + \tfrac{1}{2}O_2 \rightarrow H_2O \; (liquid)$$
$$\Delta\bar{h}_f = -285.84 \; kJ/mole$$

H_2O (g)	-241.826 kJ/mol [$\Delta_f H^\circ$ (298.15 K)]	9.905 kJ/mol [H° (298.15 K) – H° (0 K)]
H_2O (l)	-285.830 kJ/mol [$\Delta_f H^\circ$ (298.15 K)]	13.273 kJ/mol [H° (298.15 K) – H° (0 K)]

D. R. Lide, *CRC Handbook of Chemistry and Physics*, p. 5-2 (2000).

Types of Fuel Cells

	Electrolyte	Operating Temperature	Charge Carrier	Catalyst	Power
SOFC (Solid Oxide Fuel Cell)	Ceramic (YSZ)	1000˚C	O^{2-}	Perovskites	MW
MCFC (Molten Carbonate Fuel Cell)	Immobilized Liquid Molten Carbonate	650˚C	CO_3^{2-}	Ni	MW
PAFC (Phosphoric Acid Fuel Cell)	Immobilized Liquid Phosphoric Acid	200˚C	H^+	Pt	kW
PEMFC (Proton Exchange Membrane Fuel Cell)	Ion Exchange Membrane (Nafion)	80˚C	H^+ or OH^-	Pt	kW-W
DMFC (Direct Methanol Fuel Cell) + DAFC (Direct Alcohol Fuel Cell)	Ion Exchange Membrane (Nafion)	30-90˚C	H^+ or OH^-	Pt, Pt-Ru	W

Fuel-Cell Components

~1960

Anode

Cathode

Nafion Membrane

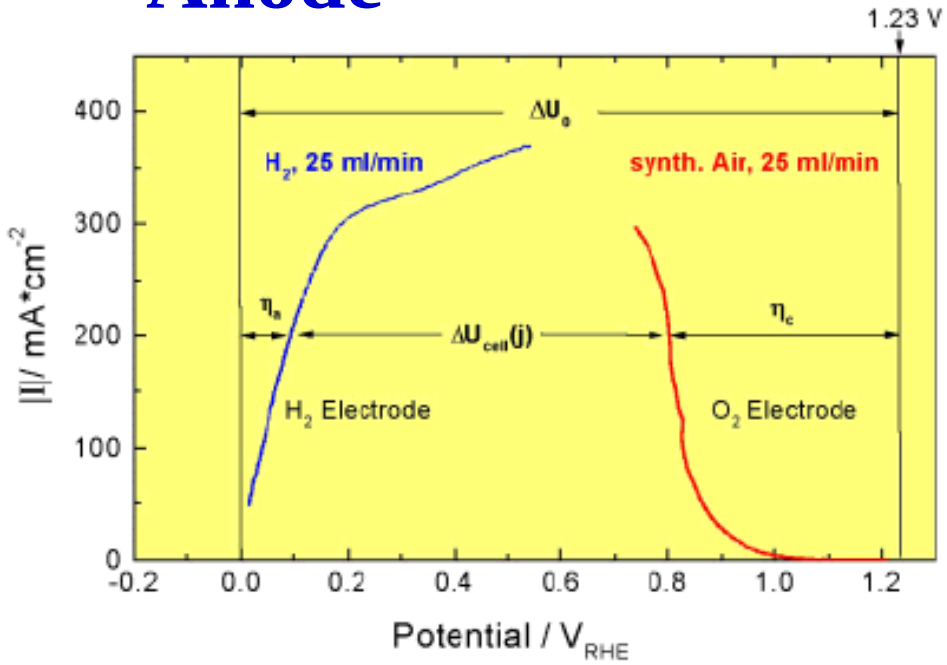

Fig. 2 The dependence of the current density versus potential for anode and cathode reaction. Measured potential dependence regarding hydrogen oxidation and oxygen reduction from air in a membrane electrode assemblie (MEA). Electrolyte: Nafion 117, Pt/C-catalysts.

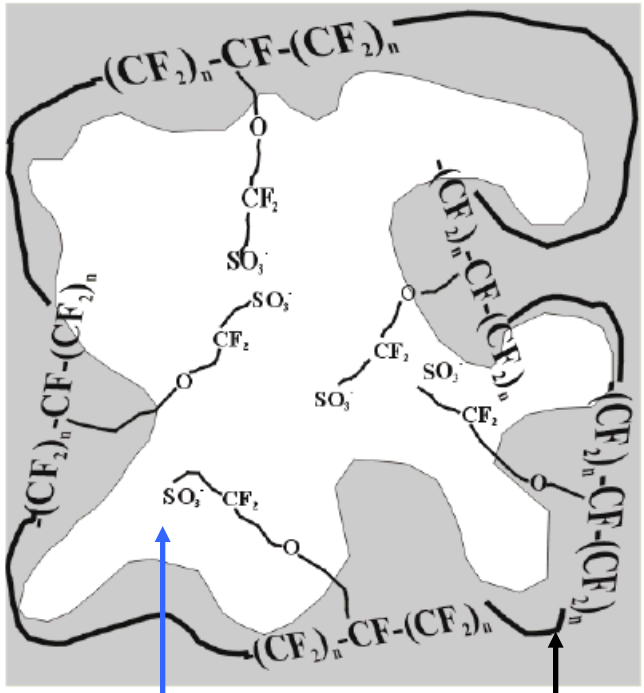

Fig. 7 The structure of Nafion showing the three different regions: the hydrophobic PTFE backbone, the hydrophilic ionic zone, and the intermediate region.

U. Stimming's Group, Technische Universität München
Fuel Cells (2001).

State of Understanding of Nafion

Kenneth A. Mauritz* and Robert B. Moore*

Department of Polymer Science, The University of Southern Mississippi, 118 College Drive #10076, Hattiesburg, Mississippi 39406-0001

Nafion ionomers were developed and are produced by the E. I. DuPont Company. These materials are generated by copolymerization of a perfluorinated vinyl ether comonomer with tetrafluoroethylene (TFE), resulting in the chemical structure given below.

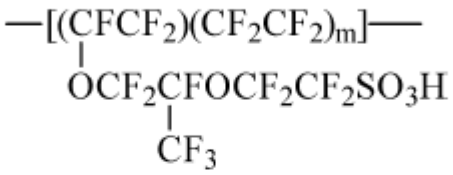

Equivalent weight (EW) is the number of grams of dry Nafion per mole of sulfonic acid groups when the material is in the acid form. This is an average EW in the sense that the comonomer sequence distribution (that is usually unknown to the investigator and largely unreported) gives a distribution in m in this formula. EW can be ascertained by acid–base titration, by analysis of atomic sulfur, and by FT-IR spectroscopy. The relationship between EW and m is EW = $100m + 446$ so that, for example, the side chains are separated by around 14 CF_2 units in a membrane of 1100 EW.

State of Understanding for Nafion

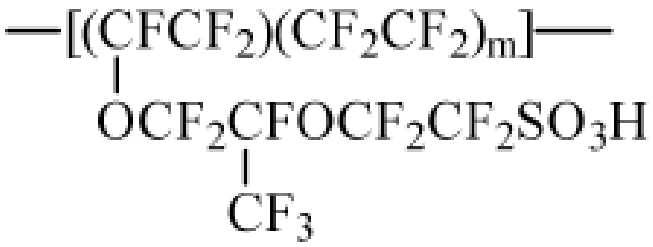

- Difficult synthetic process
- Poor conductivity at high temperature
- **Methanol crossover**
- High material cost

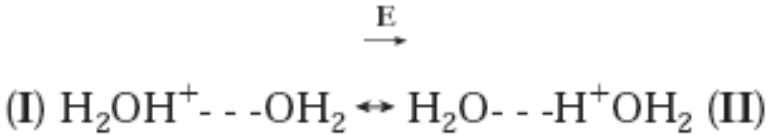

Polymer Structure

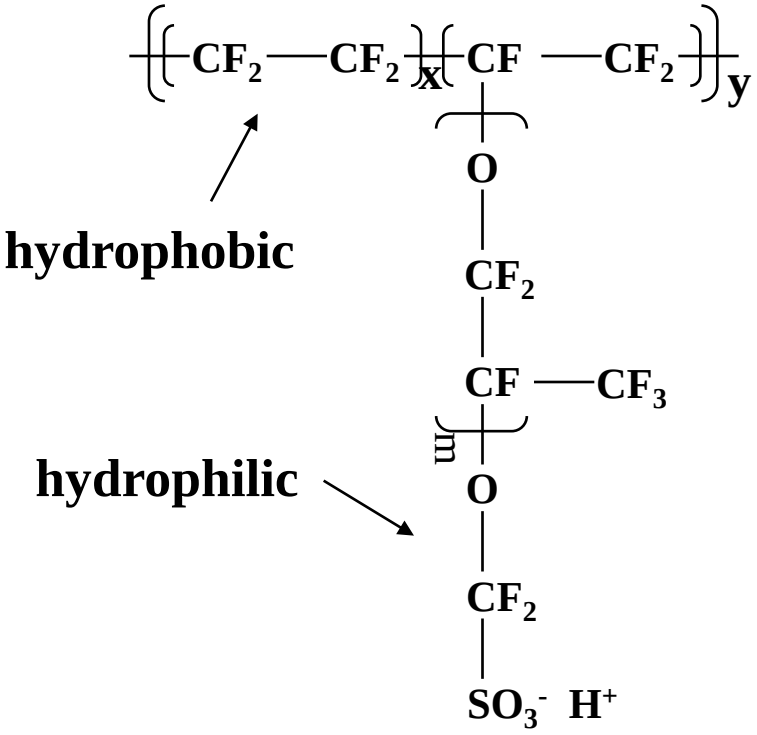

x=5, y=1000

m=0~3

K. A. Mauritz's group, The University of Southern Mississippi
Chem. Rev. (2004).

The Role of Electrocatalyst

The use of electrocatalysts serves faster kinetic paths.

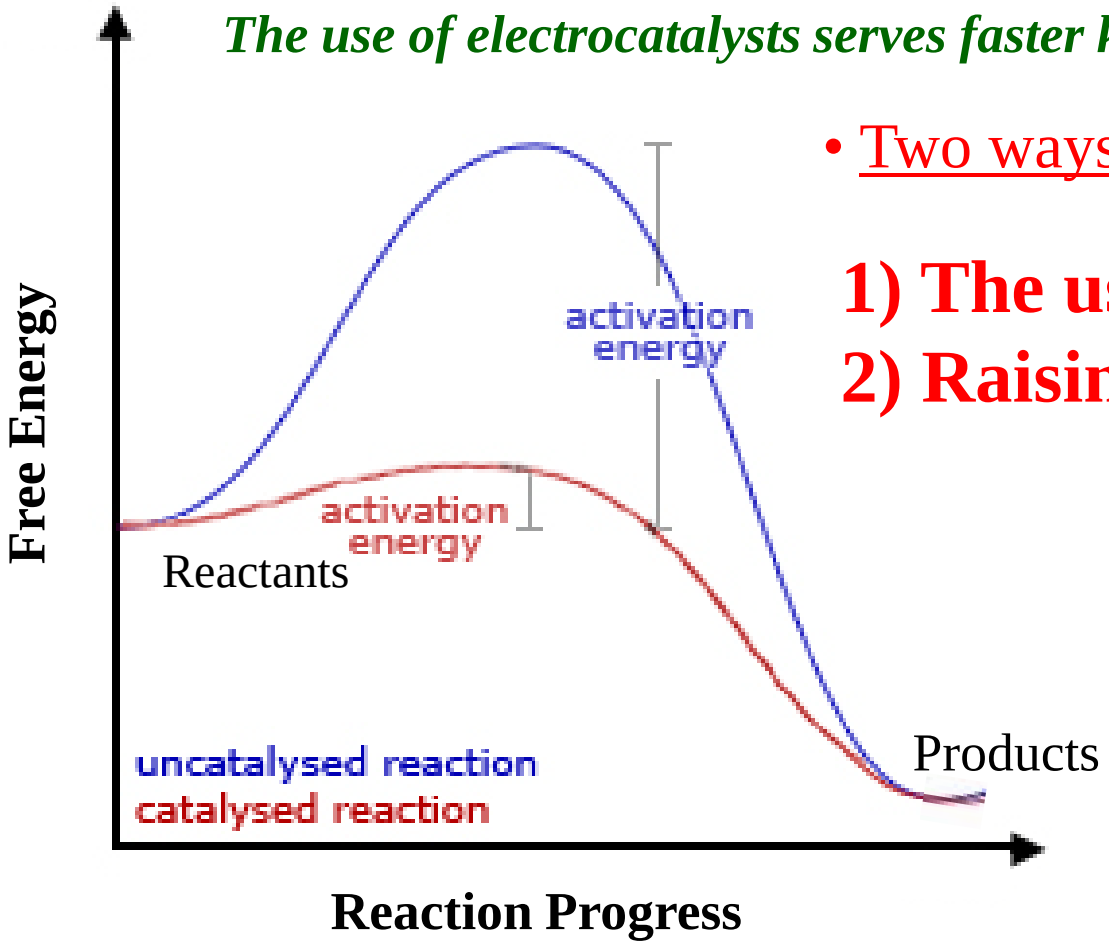

- Two ways to get over the ‘energy hill’

1) The use of catalysts.

2) Raising the temperature.

W. Vielstich, A. Lamm, and H. A. Gasteiger
Handbook of Fuel Cells, John Wiley & Sons Ltd (2003).

Electrocatalysts: Supplying Different Paths by Total-Energy Calculation

Uncatalyzed Reaction

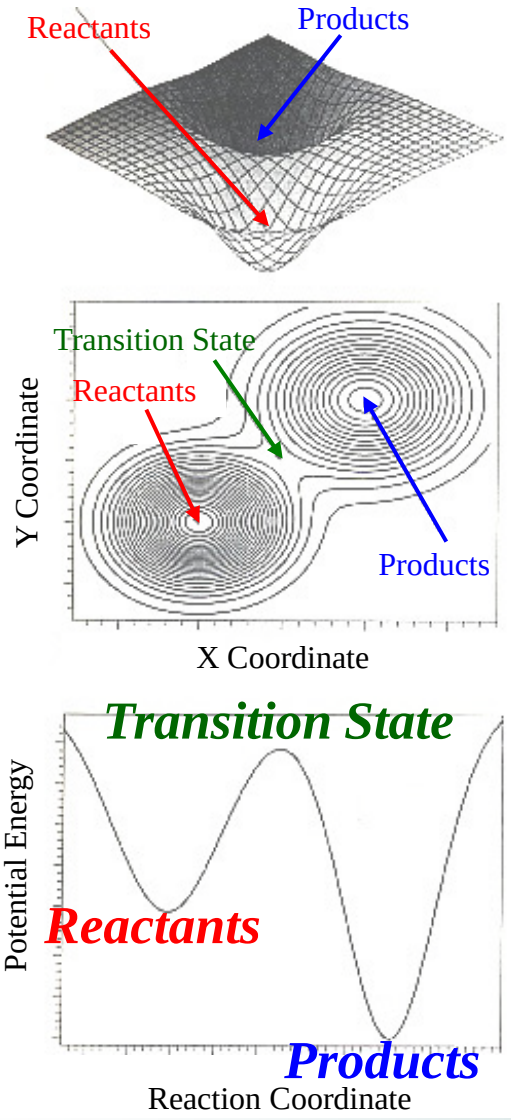

Catalyzed Reaction

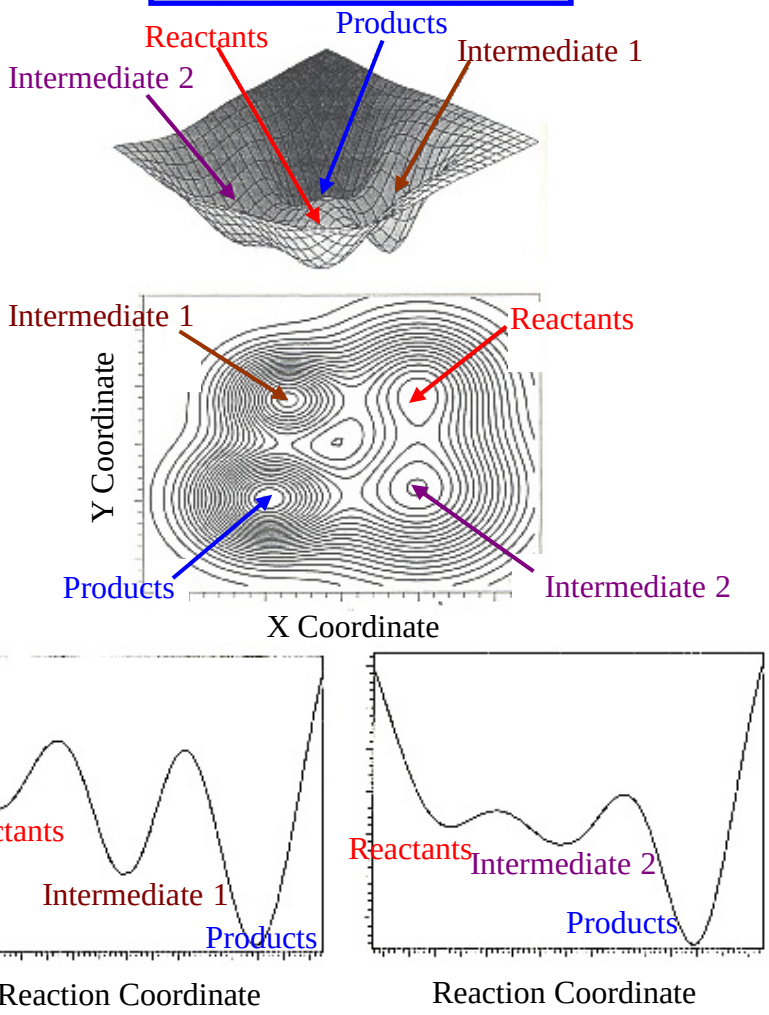

W. Vielstich, A. Lamm, and H. A. Gasteiger
Handbook of Fuel Cells, John Wiley & Sons Ltd (2003).

Reactions on Pt Catalysts

W. Vielstich, A. Lamm, and H. A. Gasteiger
Handbook of Fuel Cells, John Wiley & Sons Ltd (2003).

Hydrogen Oxidation

$Pt\text{-}H \rightarrow Pt + H^+ + e^-$

Water Oxidation

$Pt\text{-}H_2O \rightarrow Pt\text{-}OH + H^+ + e^-$

$Pt\text{-}OH \rightarrow Pt\text{-}O + H^+ + e^-$

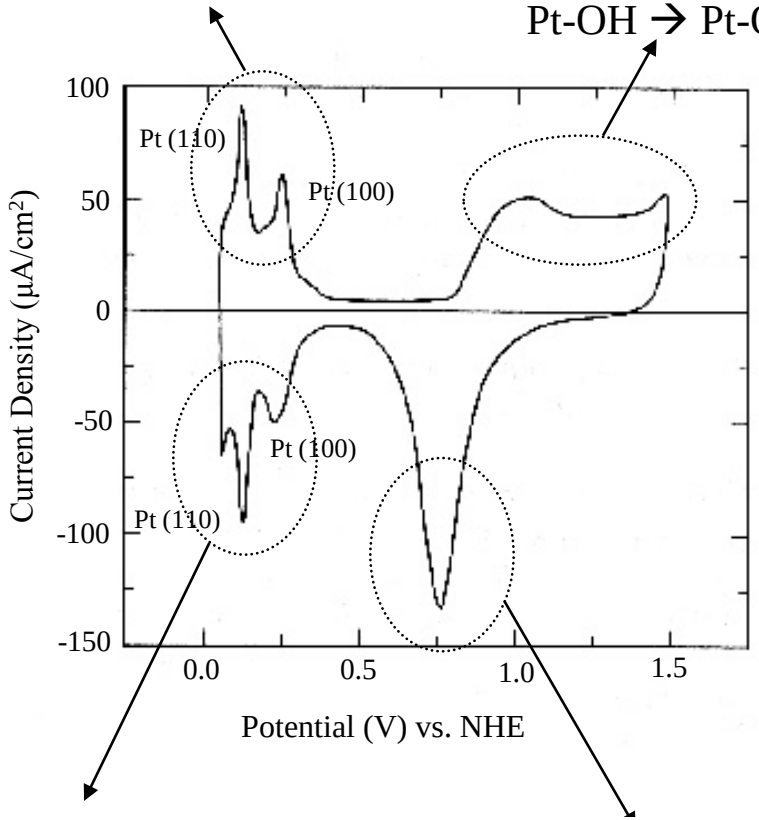

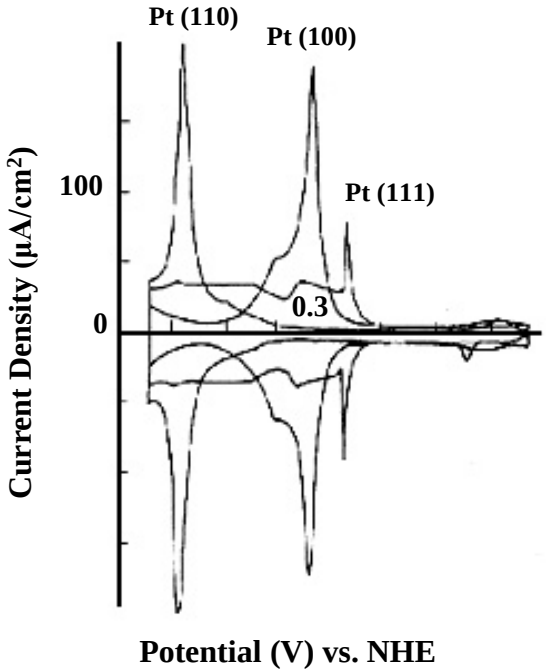

Surface Orientation Dependency (Single Crystal)

Hydrogen Reduction

$Pt + H^+ + e^- \rightarrow Pt\text{-}H$

Oxygen Reduction

$Pt\text{-}O + H^+ + e^- \rightarrow Pt\text{-}OH$

$Pt\text{-}OH + H^+ + e^- \rightarrow Pt\text{-}H_2O$

Hydrogen Oxidation Reaction (HOR) vs.

Metal-Hydrogen Bonding Energy

Exchange current

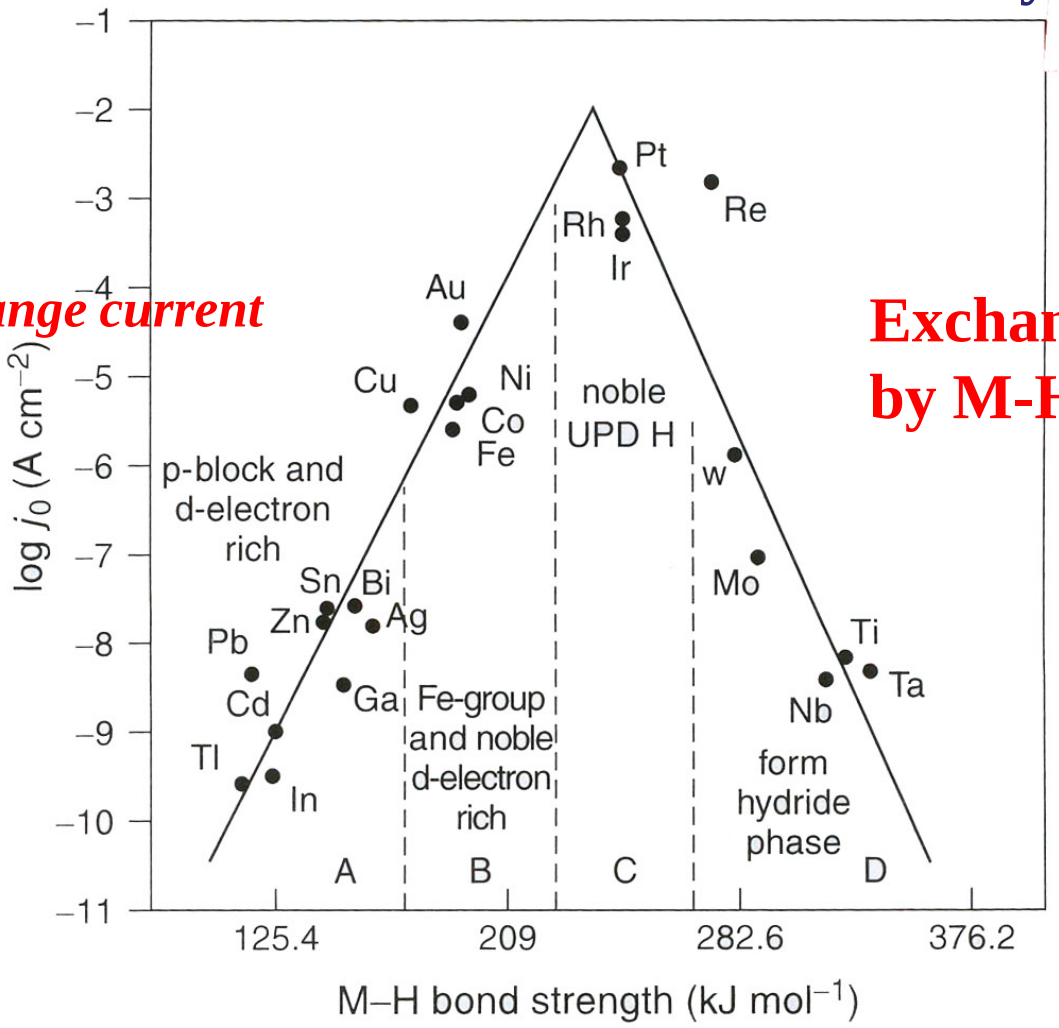

Exchange current is determined by M-H bonding strength.

W. Vielstich, A. Lamm, and H. A. Gasteiger
Handbook of Fuel Cells, John Wiley & Sons Ltd (2003).

Oxygen-Reduction Reaction (ORR) and Tafel Slope

K. E. Swider-Lyons' Group, Naval Research Laboratory
J. Electrochem. Soc. (2004).

Rotating Disk Electrodes

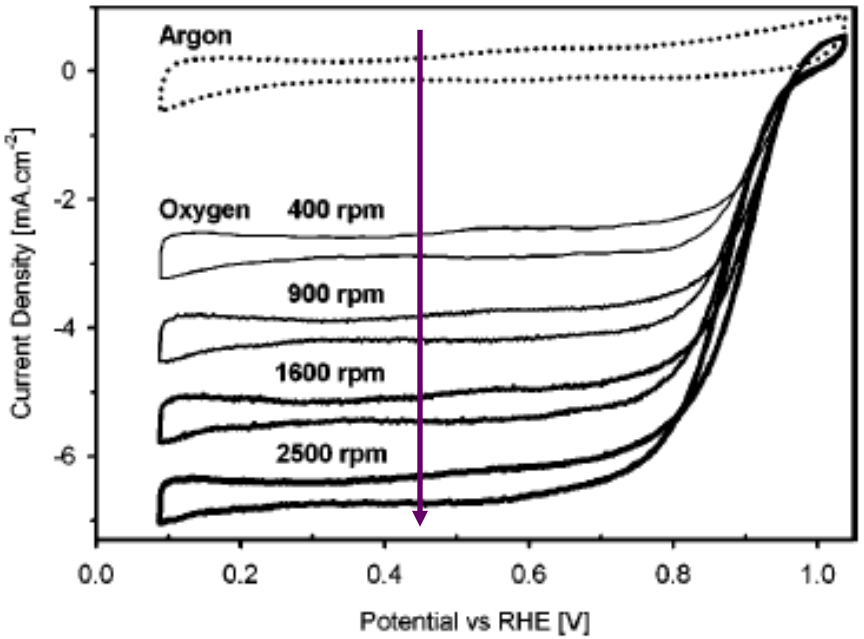

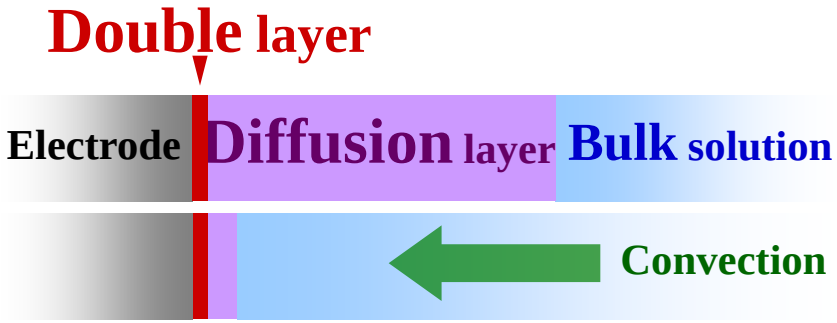

Tafel Slope

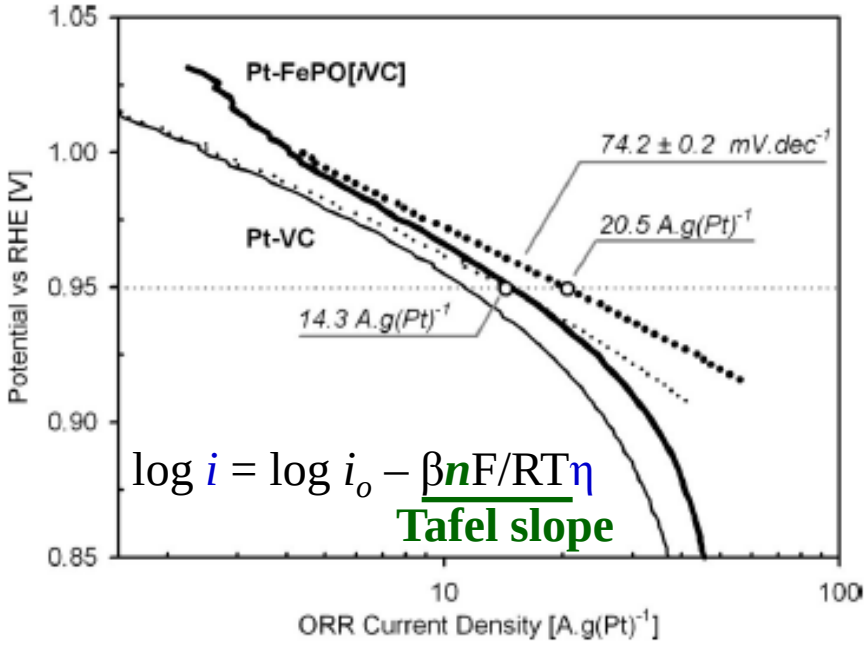

$$\log i = \log i_o - \beta n F/RT\eta$$

Tafel slope

i: current density
i_0: exchange current density
F: Faraday constant
n: the number of electrons involved in the reaction
β: symmetry constant
η: overpotential

Reaction Mechanisms of ORR

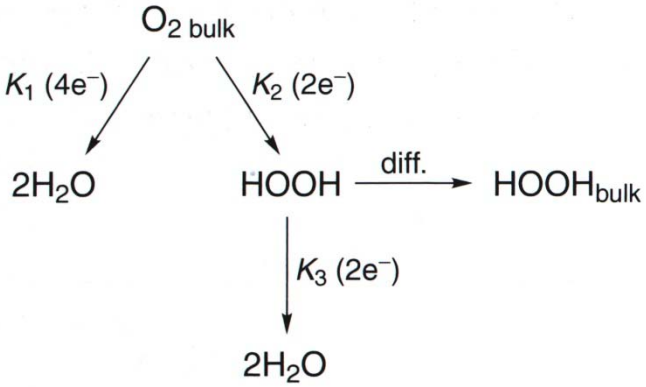

W. Vielstich, A. Lamm, and H. A. Gasteiger
Handbook of Fuel Cells, John Wiley & Sons Ltd (2003).

Four-Electron Process

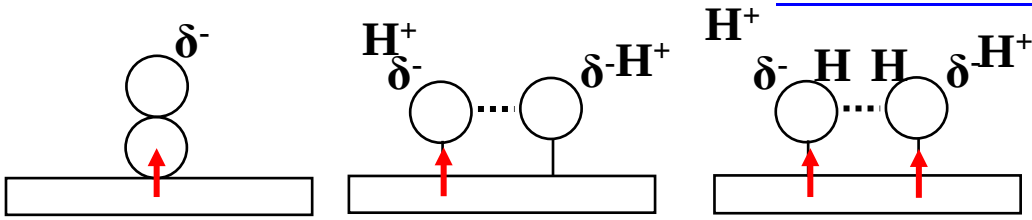

$O_2^{\delta-}$ **First Adsorption**

$2O^{\delta-}$ **Second Adsorption**

(Oxygen dissociation)

4-electron reduction of oxygen to water

$O_2 + 4e^- + 4H^+ \leftrightarrow 2H_2O$ $\quad E^0 = 1.229$ V vs. NHE

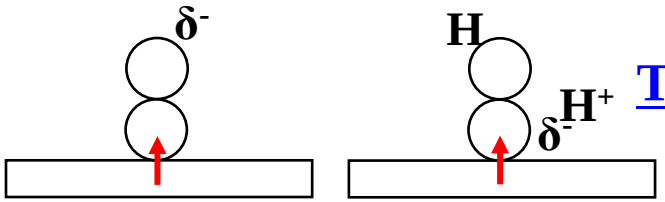

$O_2^{\delta-}$ **First adsorption**

Two-Electron Process

2-electron reduction of oxygen to peroxide (H_2O_2)

Reaction Mechanisms of ORR

ORR pathway is more complex than HOR.
Mechanisms are not known exactly.

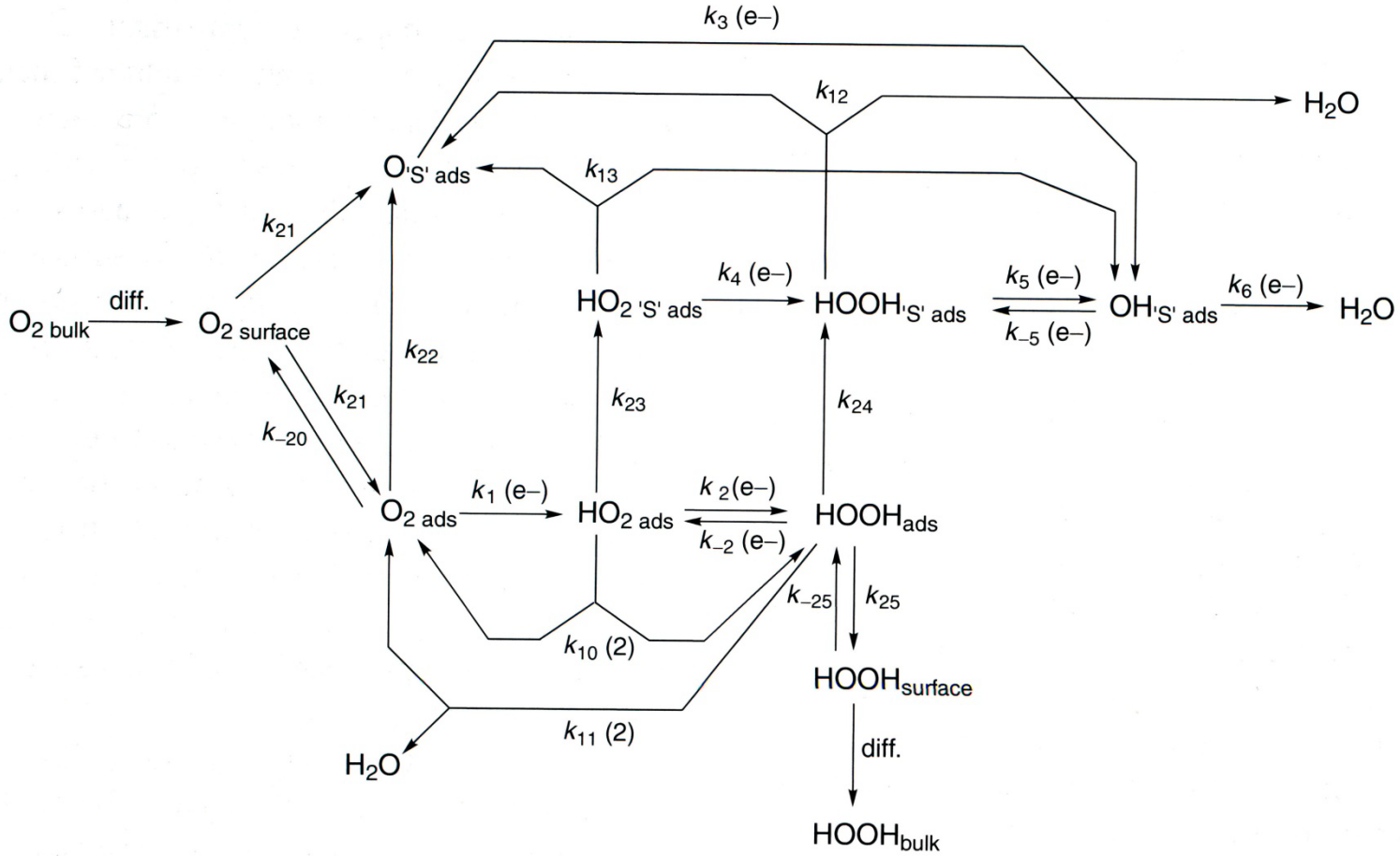

W. Vielstich, A. Lamm, and H. A. Gasteiger
Handbook of Fuel Cells, John Wiley & Sons Ltd (2003).

Mechanisms of Methanol Oxidation

$$CH_3OH + H_2O \rightarrow CO_2 + 6H^+ + 6e^- \quad E = 0.05\ V$$

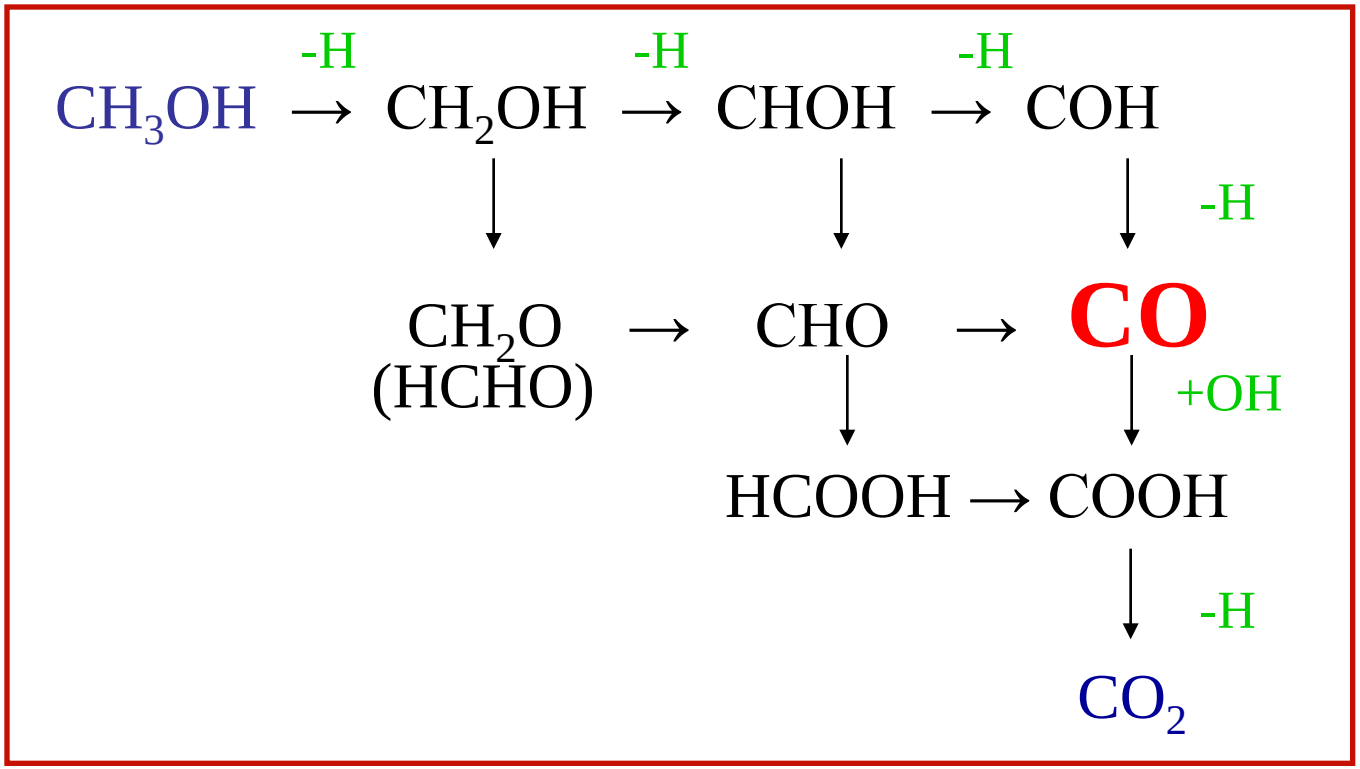

CO Tolerant Catalyst

Table 1. Effect of Pt alloying with each element on the CO tolerance at anodic H_2 oxidation.[a]

4a	5a	6a	7a		8		1b	2b	3b	4b	5b
Ti	V	Cr	Mn	Fe	Co	Ni	Cu	Zn	Ga	Ge	As
P		P	G	E	E	E	P	G		P	
Zr	Nb	Mo	Tc	Ru	Rh	Pd	Ag	Cd	In	Sn	Sb
	P	E		E		P	G		P	G	P
Hf	Ta	W	Re	Os	Ir	Pt	Au	Hg	Tl	Pb	Bi
		P					P			P	P

[a]E, no degradation; G, degradation with time; P, immediate degradation.

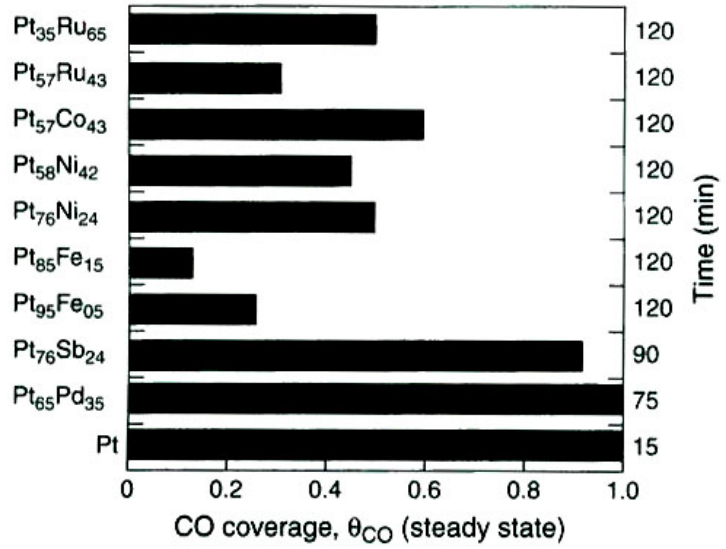

Bimetallic Function

$$(CH_3OH)_{ad} \leftrightarrow (CO)_{ad} + 4H^+ + 4e^-$$

$$\mathbf{Ru} + H_2O \leftrightarrow (OH)_{ad} + H^+ + e^-$$

$$Pt(CO)_{ad} + Ru(OH)_{ad} \leftrightarrow CO_2 + H^+ + e^-$$

W. Vielstich, A. Lamm, and H. A. Gasteiger
Handbook of Fuel Cells, John Wiley & Sons Ltd (2003).

PtRu Catalysts for Enhanced CO Oxidation

1. Bifunctional Effect

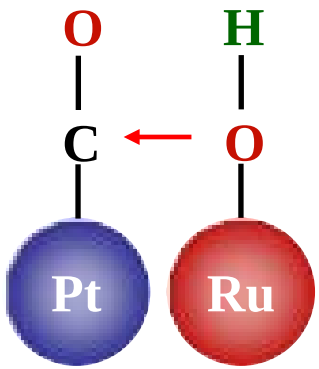

- Ru provides "active" OH in the low potential (<0.3 V)
- Pt-CO + Ru-OH ↔ Pt + Ru + CO_2 + H^+ + e^-

Watanabe's Group , *J. Electroanal. Chem.* **60**, 267 (1975).

Cairns's Group, *J. Phys. Chem.* **97**, 12020 (1993).

2. Electronic Effect

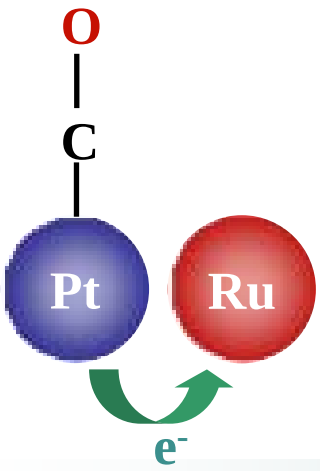

- Reduction in density of states on the Fermi level
- Reduce the bonding energy between CO and Pt

Rameshand's Group, *Chem. Mater.* **1**, 391 (1989).

Wiekowski's Group, *J. Phys. Chem.* **98**, 5074 (1994).

High-Efficiency Catalysts for Oxygen Reduction

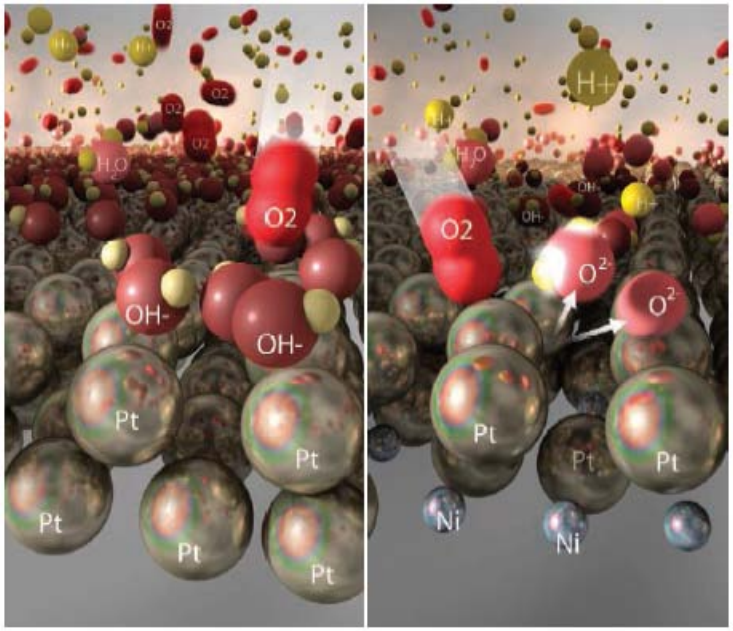

Loose grip. All-platinum electrodes (*left*) grab hydroxides (OH) tightly, preventing oxygen (O_2) from getting access to the catalyst. Adding nickel (*right*) softens this grip, speeding the desired oxygen-splitting reaction.

Nanostructure-Tailored Catalysts

N. M. Markovic's Group, Argonne National Lab.
Nature Mater. (2007).

One of the key objectives in fuel-cell technology is to improve and reduce Pt loading as the oxygen-reduction catalyst. Here, we show a fundamental relationship in electrocatalytic trends on Pt_3M (M = Ni, Co, Fe, Ti, V) surfaces between the experimentally determined surface electronic structure (the *d*-band centre) and activity for the oxygen-reduction reaction. This relationship exhibits 'volcano-type' behaviour, where the maximum catalytic activity is governed by a balance between adsorption energies of reactive intermediates and surface coverage by spectator (blocking) species. The electrocatalytic trends established for extended surfaces are used to explain the activity pattern of Pt_3M nanocatalysts as well as to provide a fundamental basis for the catalytic enhancement of cathode catalysts. By combining simulations with experiments in the quest for surfaces with desired activity, an advanced concept in nanoscale catalyst engineering has been developed.

Trends in electrocatalysis on extended and nanoscale Pt-bimetallic alloy surfaces

VOJISLAV R. STAMENKOVIC[1,2]*, BONGJIN SIMON MUN[2,3], MATTHIAS ARENZ[4], KARL J. J. MAYRHOFER[5], CHRISTOPHER A. LUCAS[5], GUOFENG WANG[6], PHILIP N. ROSS[2] AND NENAD M. MARKOVIC[1]*

[1]Materials Science Division, Argonne National Laboratory, Argonne, Illinois 60439, USA
[2]Materials Sciences Division, Lawrence Berkeley National Laboratory, University of California, Berkeley, California 94720, USA
[3]Department of Applied Physics, Hanyang University, Ansan, Kyunggi-Do 426-791, Korea
[4]Technical University of Munich, 80333 Munich, Germany
[5]Oliver Lodge Laboratory, Department of Physics, University of Liverpool, Liverpool L69 7ZE, UK
[6]Department of Chemistry and Physics, University of South Carolina, Aiken, South Carolina 29801, USA
*e-mail: vrstamenkovic@anl.gov; nmmarkovic@anl.gov

Published online: 18 February 2007; doi:10.1038/nmat1840

One of the key objectives in fuel-cell technology is to improve and reduce Pt loading as the oxygen-reduction catalyst. Here, we show a fundamental relationship in electrocatalytic trends on Pt_3M (M = Ni, Co, Fe, Ti, V) surfaces between the experimentally determined surface electronic structure (the *d*-band centre) and activity for the oxygen-reduction reaction. This relationship exhibits 'volcano-type' behaviour, where the maximum catalytic activity is governed by a balance between adsorption energies of reactive intermediates and surface coverage by spectator (blocking) species. The electrocatalytic trends established for extended surfaces are used to explain the activity pattern of Pt_3M nanocatalysts as well as to provide a fundamental basis for the catalytic enhancement of cathode catalysts. By combining simulations with experiments in the quest for surfaces with desired activity, an advanced concept in nanoscale catalyst engineering has been developed.

Comparison of Several Pt_3M Alloys

N. M. Markovic's Group, Argonne National Lab.
Nature Mater. (2007).

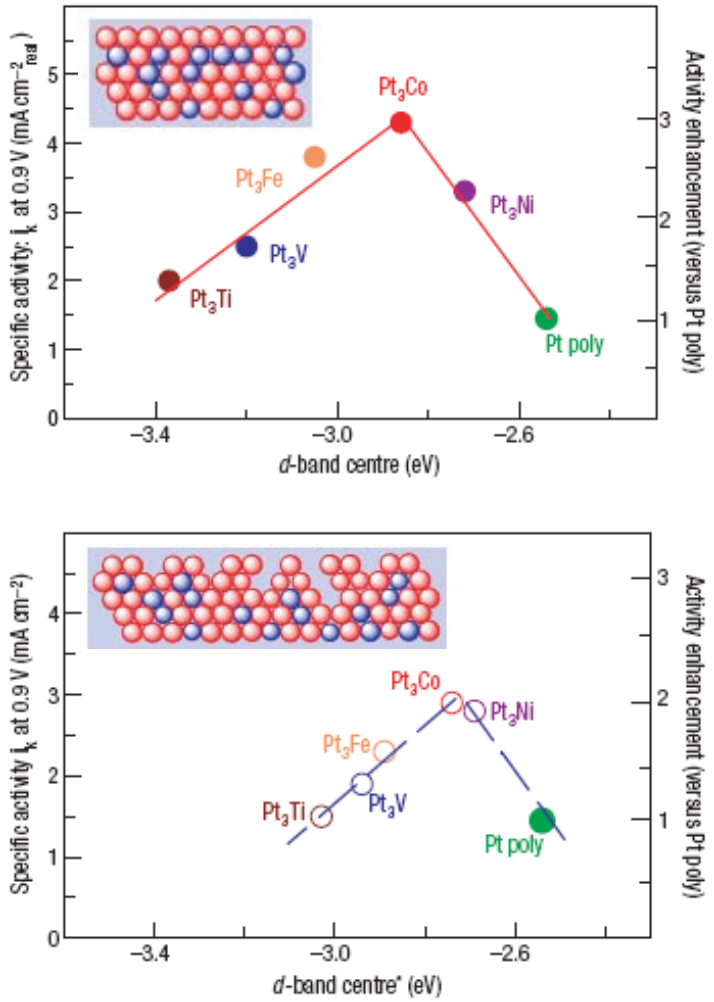

Figure 4 Relationships between the catalytic properties and electronic structure of Pt_3M alloys. a,b, Relationships between experimentally measured specific activity for the ORR on Pt_3M surfaces in 0.1 M $HClO_4$ at 333 K versus the *d*-band centre position for the Pt-skin (**a**) and Pt-skeleton (**b**) surfaces. **b** shows the *d*-band centre values* established in UHV, which may deviate in the electrochemical environment due to dissolution of non-Pt atoms.

Pt_3Co Nanoparticle

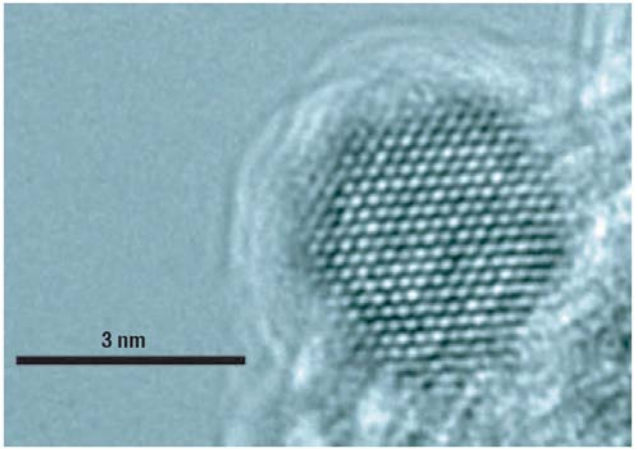

High-resolution transmission electron micrograph of a Pt_3Co nanoparticle.

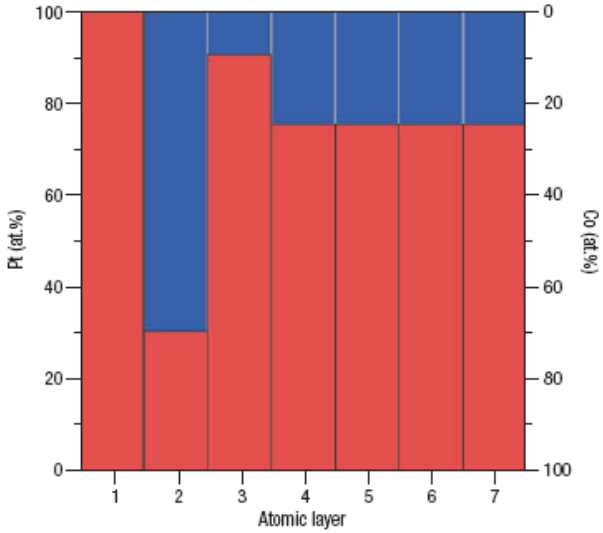

Concentration profile for the Pt_3Co nanoparticle obtained from calculations.

Vital Role of Moisture in the Catalytic Activity

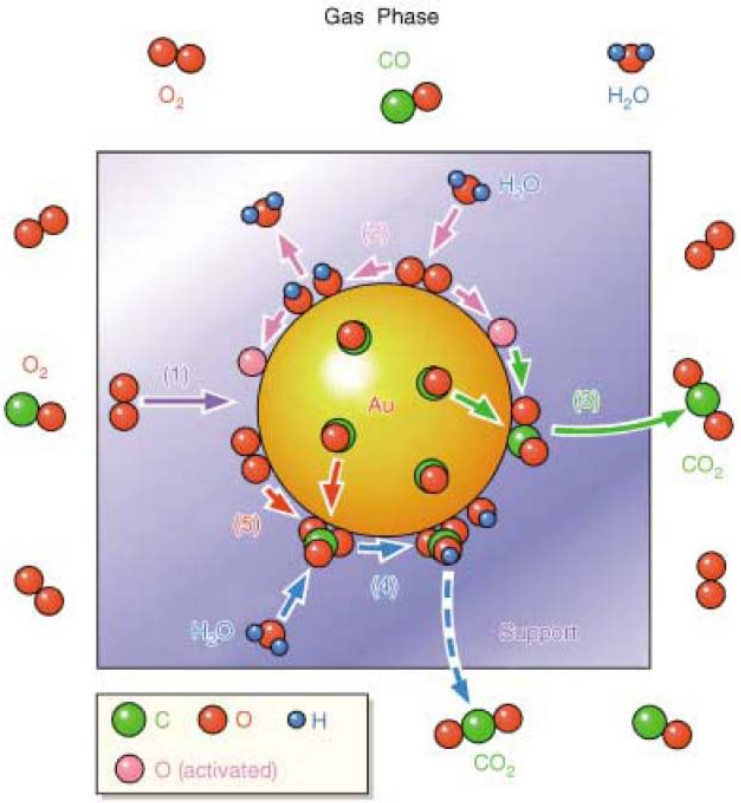

Figure 5. Schematic model (top view) for CO oxidation under the coexistence of moisture. Arrows indicate the processes on the catalyst surface: (1) oxygen diffusion from the support surface, (2) activation of oxygen, (3) production of CO_2, (4) decomposition of carbonate and (5) formation of carbonate. The numbers except for (1) correspond to Equations (2)–(5) in Scheme 1.

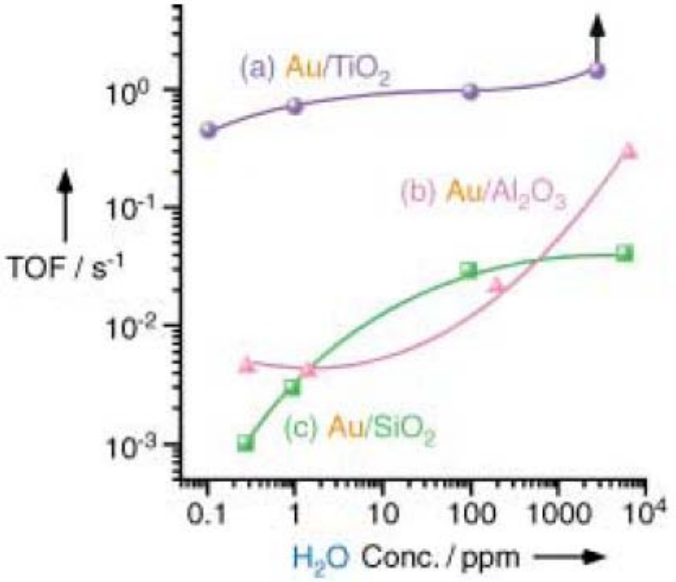

Figure 2. Turnover frequencies per surface gold atom at 273 K for CO oxidation over a) Au/TiO_2, b) Au/Al_2O_3 and c) Au/SiO_2 as a function of moisture concentration. Upright arrow indicates the saturation of CO conversion.

Masakazu Date's Group, AIST (Japan)
Angew. Chem. Int. Ed. (2004).

Activation of oxygen by water

$$O_2(p) + H_2O(s) \longrightarrow O^*(p) + 2OH(p) \quad (2a)$$

$$2OH(p) \longrightarrow O^*(p) + H_2O(s) \quad (2b)$$

$$CO(Au) + O^*(p) \longrightarrow COO(p) \longrightarrow CO_2(g) \quad (3)$$

(p): interface, (s): support, (g): gas

Heterogeneous Catalysis

Vital Role of Moisture in the Catalytic Activity of Supported Gold Nanoparticles**

Masakazu Daté, Mitsutaka Okumura, Susumu Tsubota, and Masatake Haruta*

Why can inert gold become catalytically active only when dispersed in the form of nanoparticles?—This simple question has attracted growing interest in the field of not only catalytic and industrial chemistry,[1–4] but also cluster and theoretical science.[5–7] To answer this question, CO oxidation has been intensively studied as a model reaction.[8–14] The reaction is known to be greatly influenced by moisture in the reactant gas.[10,15] However, only a few recent studies discuss the reaction mechanisms taking water into account.[16,18] Even in these studies on the effect of moisture, for practical reasons, the addition of water vapor has been examined only at high concentrations.

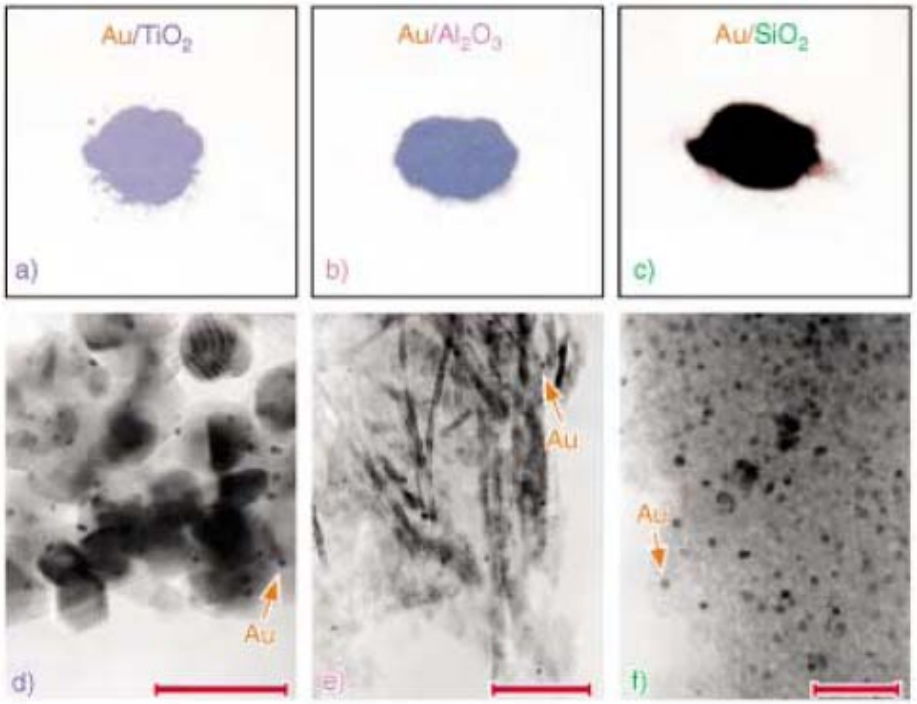

Figure 1. Photographs of a) Au/TiO_2 (violet in appearance), b) Au/Al_2O_3 (grayish blue) and c) Au/SiO_2 (dark red) catalyst samples along with TEM micrographs of d) Au/TiO_2, e) Au/Al_2O_3 and f) Au/SiO_2. Scales in the micrographs indicate 50 nm.

CO Oxidation Experiments with O_2 and partial H_2O

Journal of The Electrochemical Society, **153** (9) A1702-A1707 (2006)
0013-4651/2006/153(9)/A1702/6/$20.00 © The Electrochemical Society

Enhanced Oxygen Reduction Activity in Acid by Tin-Oxide Supported Au Nanoparticle Catalysts

Wendy S. Baker,[a] Jeremy J. Pietron,[a] Margaret E. Teliska,[a,*] Peter J. Bouwman,[a] David E. Ramaker,[b,*] and Karen E. Swider-Lyons[a,*,z]

[a]*Naval Research Laboratory, Washington, DC 20375, USA*
[b]*Department of Chemistry, George Washington University, Washington, DC 20052, USA*

Gold nanoparticles supported on hydrous tin-oxide ($Au–SnO_x$) are active for the four-electron oxygen reduction reaction in an acid electrolyte. The unique electrocatalytic of the Au–SnO is confirmed by the low amount of peroxide detected with rotating ring-disk electrode voltammetry and Koutecký-Levich analysis. In comparison, 10 wt % Au supported on Vulcan carbon and SnO_x catalysts both produce significant peroxide in the acid electrolyte, indicating only a two-electron reduction reaction. Characterization of the $Au–SnO_x$ catalyst reveals a high-surface area, amorphous support with 1.7 nm gold metal particles. The high catalytic activity of the Au–SnO is attributed to metal support interactions. The results demonstrate a possible path to non-Pt catalysts for proton exchange membrane fuel cell cathodes.
 [DOI: 10.1149/1.2216527]

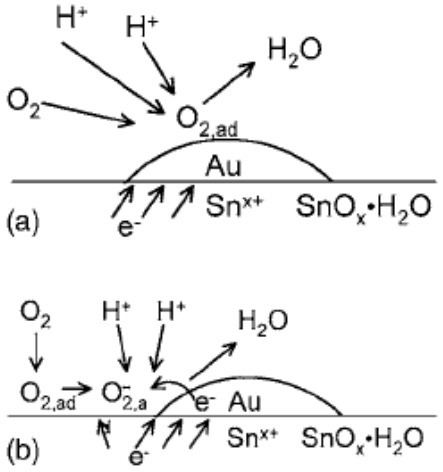

Figure 5. Notional mechanisms for the improved ORR activity of Au on hydrous tin oxide in acid. (a) Electronic effect where the Au reacts with the electron donating Sn^{2+}, resulting in an improvement of O_2 adsorption on metal, allowing the ORR, and (b) bifunctional mechanism whereby oxygen adsorbs on the hydrous tin oxide as O_2^- and is converted to hydroxyl groups, which are reduced to water on the Au.

Tin-Oxide Supported Au Nanoparticle Catalysts

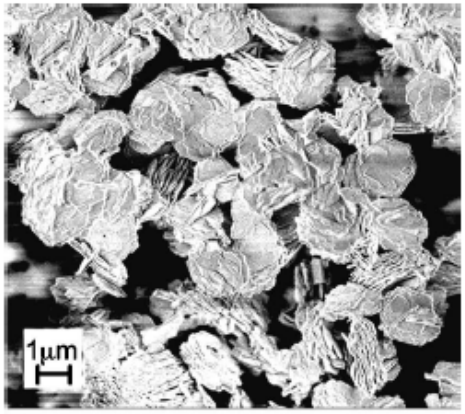

(a)

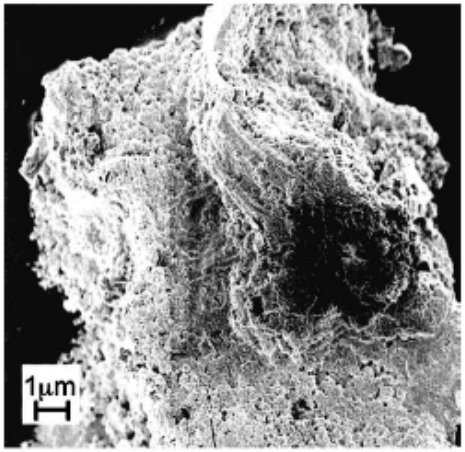

(b)

SnO_x
~ partly amorphous
~ alkaline nature

Au
~ 1.7 nm

Figure 1. SEMs of (a) SnO $[Sn_{12}Cl_{16}(OH_{14})O_6]$ precursor and (b) Au–SnO catalyst powders.

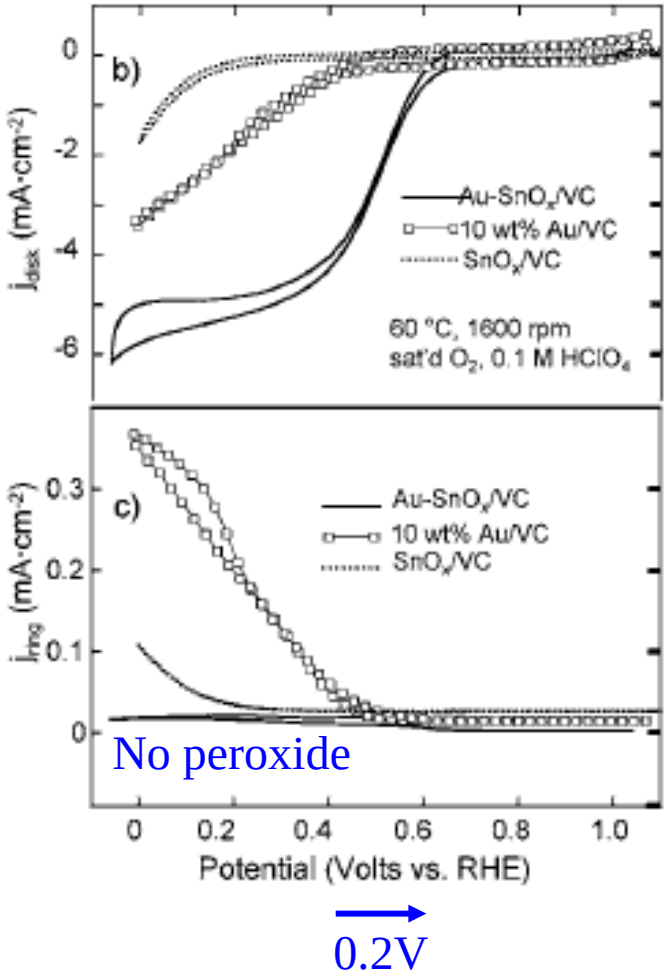

Figure 2. CV in acid for (a) Au–SnO_x/VC activation, Au loading 0.04 mg/cm^2, scan rate 5 mV/s, (b) Au–SnO_x/VC, SnO_x/VC, and 10 wt % Au/VC RDE data, and (c) Au–SnO_x/VC, SnO_x/VC, and 10 wt % Au/VC, RRDE data, E_{ring} = 1.1 V, scan rate 20 mV/s. Au loading where applicable: 0.1 mg/cm^2.

K. E. Swider-Lyons' Group, Naval Research Laboratory
J. Electrochem. Soc. (2006).

Modifying Catalytic Reactivity by Surface Dealloying

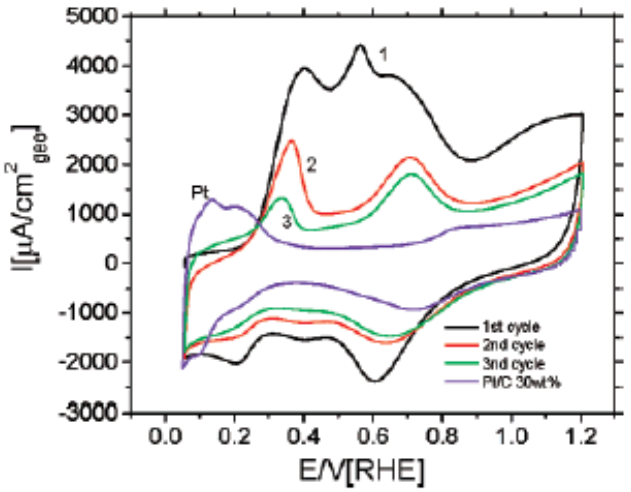

Figure 4. Initial three cyclic voltammetric (CV) profiles (1,2,3) of a Pt_{25}-Cu_{75} precursor catalyst (annealed at 600 C) during electrochemical dealloying at 100 mV/s. For comparison, the CV of a Pt standard catalyst is shown in blue.

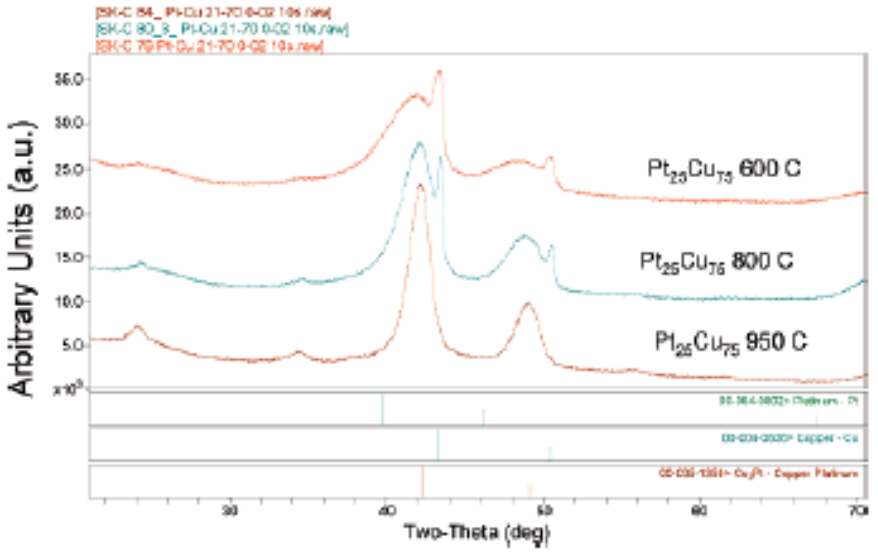

Figure 3. X-ray diffraction profiles of carbon-supported $Pt_{25}Cu_{75}$ precursor catalysts annealed at three different temperatures.

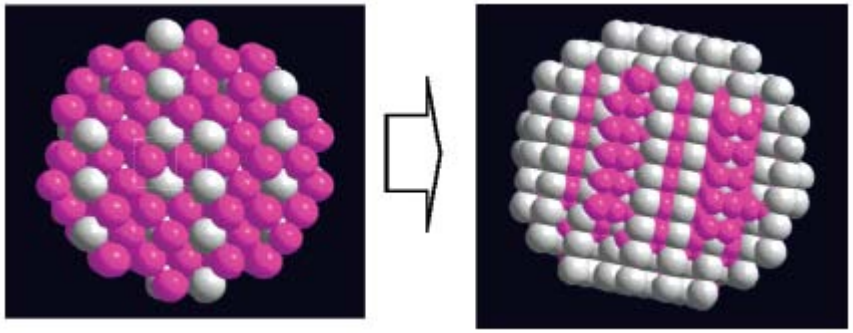

Figure 5. Electrochemical dealloying of Cu near the surface of a Cu rich Pt−Cu alloy precursor results in a core−shell particle structure.

Peter Strasser's Group, University of Houston
J. Am. Chem. Soc. (2007).

Electrocatalysis on Bimetallic Surfaces: Modifying Catalytic Reactivity for Oxygen Reduction by Voltammetric Surface Dealloying

Shirlaine Koh and Peter Strasser*

Department of Chemical and Biomolecular Engineering, University of Houston, Houston, Texas 77204

Received July 5, 2007; E-mail: pstrasser@uh.edu

The surface electrocatalytic reactivity of noble metals, for instance Pt, has frequently been modified by alloying Pt with less noble metal atoms within the top surface and/or subsurface layer.[1,2] Monolayers of pure Pt deposited on top of non-Pt substrates also showed significantly altered surface catalytic reactivity.[3] Here, we report a distinctly different synthetic strategy to modify the surface reactivity of Pt. The synthesis involves electrochemical surface dealloying, that is, selective electrodissolution, of non-noble metal atoms from bimetallic precursors. In particular, we report on significant activity enhancements for the oxygen reduction reaction (ORR) after Cu dealloying from carbon-supported Pt−Cu alloy nanoparticle electrocatalysts. After removal of Cu atoms from the surface region, the resulting particle catalysts showed previously unachieved 4−6-fold activity improvements over pure Pt.[4] Pt has been the ORR electrocatalyst of choice for decades, yet the search for more active electrocatalysts continues to be a key scientific and technological challenge in the area of electrochemical energy conversion and has become a "conditio sine qua non" in polymer electrolyte membrane fuel cell research.

The electrocatalytic activity of dealloyed Pt−Cu catalysts for

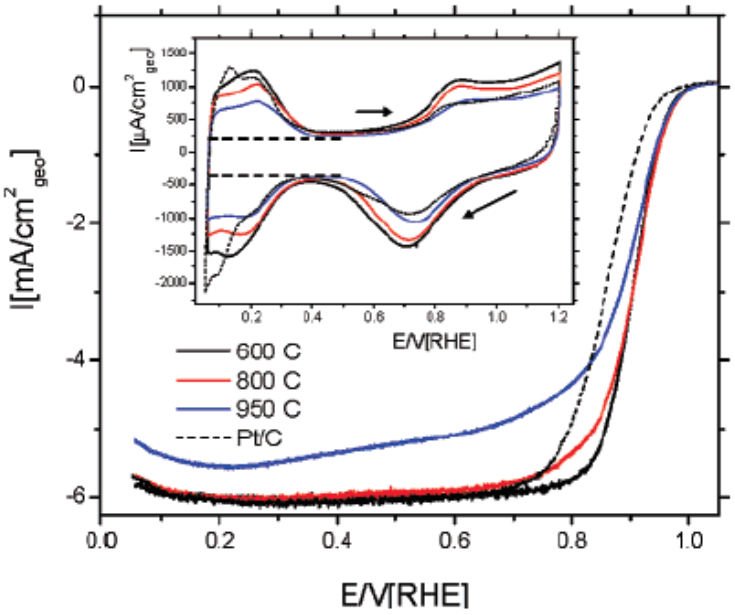

Figure 1. Sweep voltammetry of dealloyed $Pt_{25}Cu_{75}$ catalysts, annealed at 600 °C (black), 800 °C (red), 950 °C (blue), compared to Pt (dotted). The inset shows the cyclic voltammograms of the catalysts in O_2 free electrolyte. The horizontal black dotted line indicates the positive and negative capacitance currents. Arrows indicate scan directions.

Electrocatalytic Oxidation of Small Carbohydrate Fuels at Pt−Sn Modified Electrodes

María J. González,† Christopher T. Hable, and Mark S. Wrighton*

Department of Chemistry, Massachusetts Institute of Technology, Cambridge, Massachusetts 02139

Received: June 29, 1998; In Final Form: September 20, 1998

Alternative Fuels

The electrocatalytic oxidations of water-soluble alcohols and diols and some other small organic molecules (MeOH, EtOH, 2-fluoroethanol, 2,2-difluoroethanol, 2,2,2-trifluoroethanol, $CH_2(OH)_2$, ethylene glycol, *n*-PrOH, *i*-PrOH, 1,4-butanediol, 1,3-propanediol, 1,2-propanediol, *t*-BuOH, neopentyl alcohol, benzyl alcohol, 2-Me-1-PrOH, formic acid, acetaldehyde, acetic acid, propionaldehyde, propionic acid, acetone, glycolaldehyde, glyoxal, glycolic acid, glyoxylic acid, oxalic acid) have been compared in aqueous 0.5 M H_2SO_4 at C and Au electrodes modified with an electrodeposited Pt−Sn catalyst at low (−0.1 to 0.5 V vs SCE) potentials. The Pt−Sn catalyst is electrochemically deposited and forms as a smooth deposit on Au electrodes. At a catalyst loading of ~0.5 mg/cm^2 the electrodeposition of the Pt−Sn catalyst results in formation of adherent ~0.8 μm size particles on C electrodes. In general, for organic molecules containing only C, H, and O with two or more carbon atoms, the presence of H atoms on both the α- and β-carbon results in a relatively negative potential for onset of catalytic current (usually between −0.1 and −0.2 V vs SCE) at Pt−Sn compared to Pt alone. Of the alcohols and diols studied, formaldehyde (which exists in aqueous solutions as the hydrated form, $CH_2(OH)_2$) shows the highest electrocatalytic currents at the Pt−Sn catalyst. The ultimate product, via HCOOH, is CO_2. EtOH is oxidized only to acetic acid on Pt−Sn electrodes. The EtOH and *n*-PrOH oxidation yields, determined by exhaustive electrolysis, are 4 e$^-$ per molecule, while *i*-PrOH yields only 2 e$^-$ per molecule. We confirmed the generation of acetic acid, propionic acid, and acetone as the final products for the oxidations of EtOH, *n*-PrOH, and *i*-PrOH, respectively, by ^{13}C NMR and/or GCMS. The electron yield of the oxidation of ethylene glycol at Pt−Sn surfaces is only 4 e$^-$ per molecule instead of the value of 8 e$^-$ per molecule expected for the oxidation of ethylene glycol to oxalic acid. Glycolic acid (CHOCOOH) is the oxidation product by GCMS. This substance is not electrocatalytically oxidized on Pt−Sn at potentials negative of ~ +0.4 V vs SCE in comparison to the −0.1 V vs SCE onset for ethylene glycol oxidation. MeOH, the molecule with the highest electron yield on Pt−Sn (6 e$^-$ per molecule), unfortunately shows the most positive potential onset for oxidation among the group of alcohols compared in this study, while the two intermediates along the path of oxidation to CO_2, formaldehyde, and formic acid are oxidized on Pt−Sn at very negative potentials compared to MeOH. Thus, the conversion of MeOH to formaldehyde is the efficiency-determining step in the oxidation of MeOH to CO_2.

Alternative Fuels

Mark S. Wrighton's Group, Massachusetts Institute of Technology
J. Phys. Chem. B (1998).

Requirements

- Low to no toxicity
- Facility to store and handle safely
- High energy density
- Oxidation potential close to the H^+/H_2 couple

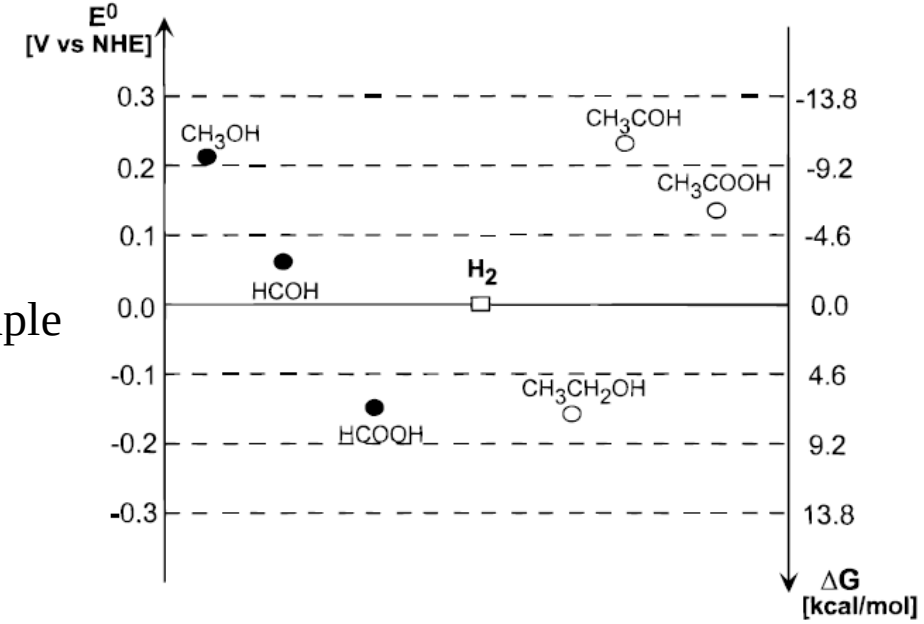

Figure 1. Equilibrium potentials and free energies for the 2 e^- oxidation of some organic molecules.

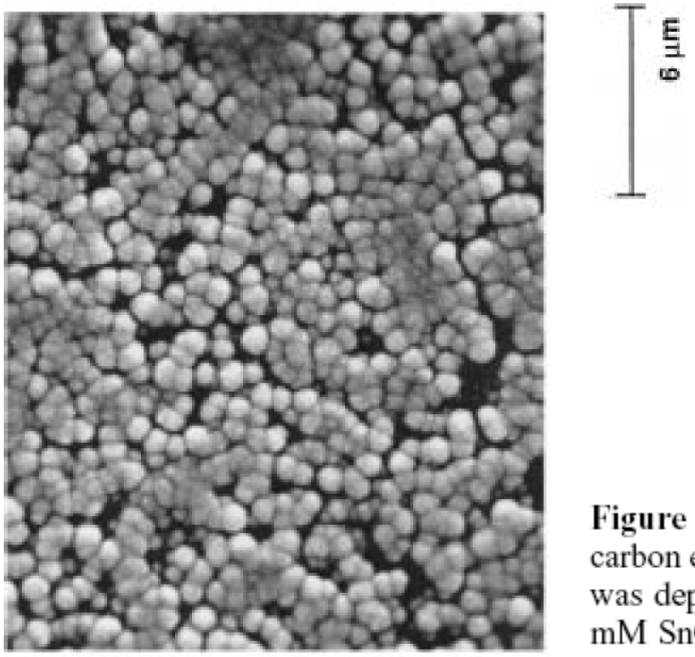

Figure 2. SEM micrographs of Pt−Sn catalyst deposited on a glassy carbon electrode. The catalyst loading is about 0.5 mg/cm^2. The catalyst was deposited from 0.5 M H_2SO_4 containing 12 mM K_2PtCl_6 and 28 mM $SnCl_4 \cdot 5H_2O$.

Mark S. Wrighton's Group, Massachusetts Institute of Technology
J. Phys. Chem. B (1998).

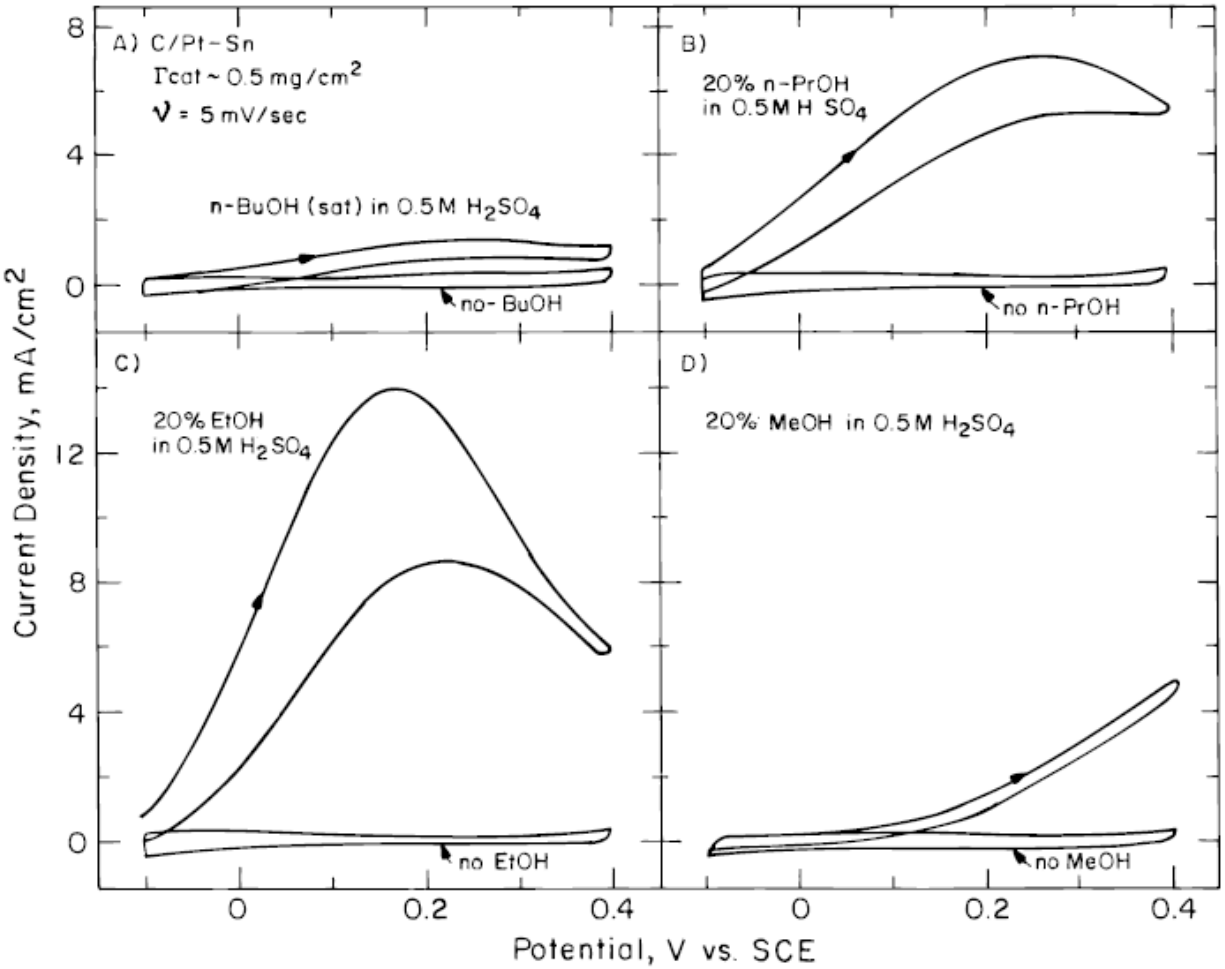

Figure 7. Comparison of the reactivities of primary alcohols with different C-chain lengths. The concentration of the fuel is 20 vol % in 0.5 M H_2SO_4 in each case. The scan rate is 5 mV/s.

Electrocatalytic Oxidation of Methanol and Ethanol: A Comparison of Platinum–Tin and Platinum–Ruthenium Catalyst Particles in a Conducting Polyaniline Matrix

Christopher T. Hable and Mark S. Wrighton*

Department of Chemistry, Massachusetts Institute of Technology, Cambridge, Massachusetts 02139

Received October 1, 1992®

A method is described for preparing polyaniline/Pt–Ru assemblies that are effective catalysts for electrochemical oxidation of MeOH or EtOH in aqueous H_2SO_4. The Pt–Ru particles have been deposited into polyaniline by electrochemical deposition from aqueous H_2SO_4 containing Pt(IV) and Ru(III) from addition of K_2PtCl_6 and $K_2RuCl_5 \cdot xH_2O$, respectively. The activity of the polyaniline/Pt–Ru assemblies for MeOH or EtOH oxidation is higher than that of polyaniline-coated electrodes modified with Pt alone. For the polyaniline/Pt–Ru system, high catalytic activity is observed for Pt–Ru particles that are codeposited from solutions containing from ~0.5 to 2 mM Ru(III) when a 3 mM Pt(IV) solution is used. Characterization of the electrodes by SEM shows that the codeposition procedure yields roughly spherical catalyst particles 300–400 nm in diameter dispersed throughout the polyaniline. XPS analysis shows Ru to be present in two different oxidation states, most likely Ru(0) and Ru(IV). The Pt–Ru catalyst is compared to a Pt–Sn catalyst which can also be dispersed in a polyaniline matrix. For electrodes prepared from 3 mM Pt(IV) with an appropriate amount of Sn(IV) or Ru(III), the Pt–Ru catalyst is better for MeOH oxidation than the Pt–Sn catalyst, because it is more reproducible. Both catalysts show a significant (and similar) temperature dependence for MeOH or EtOH oxidation. For EtOH oxidation the Pt–Sn catalyst is superior to the Pt–Ru catalyst, and the activity of Pt–Sn at low potentials, where polyaniline is nonconducting, is limited by the resistivity of the polyaniline film. For EtOH oxidation the initial product is acetaldehyde which, unfortunately, degrades the conductivity of polyaniline. Oxidation of MeOH occurs at more positive potentials and does yield CO_2, though formaldehyde, an intermediate product, in aqueous acid also degrades the conductivity of polyaniline.

Pt-Ru vs. Pt-Sn

Scheme I. Incorporation of Catalyst into a Polyaniline Matrix

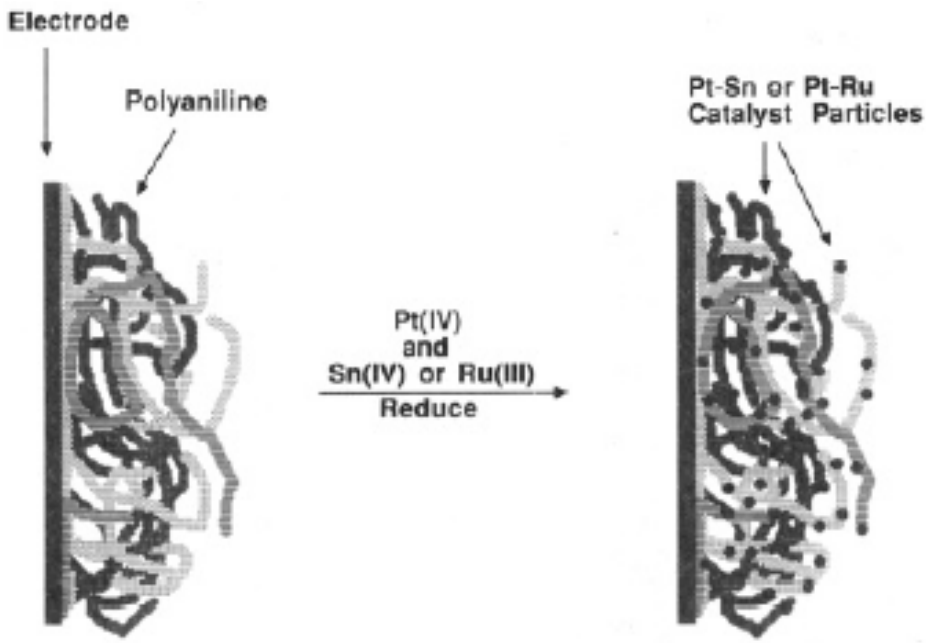

Mark S. Wrighton's Group, Massachusetts Institute of Technology
Langmuir (1993).

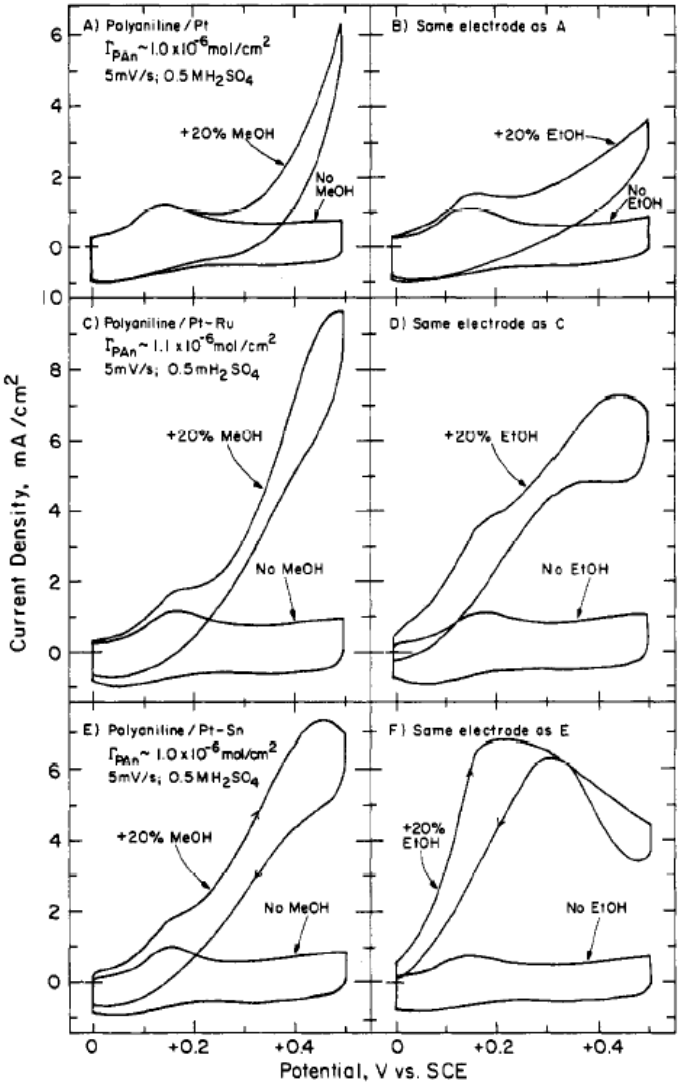

Figure 9. A comparison of MeOH oxidation and EtOH oxidation on polyaniline/Pt, polyaniline/Pt–Ru, and polyaniline/Pt–Sn electrodes. The polyaniline coverage is 1×10^{-6} mol/cm^2 and the catalyst loading is 0.5 mg/cm^2 for each electrode.

Nanoporous Pt-Based Catalysts

PtO_2

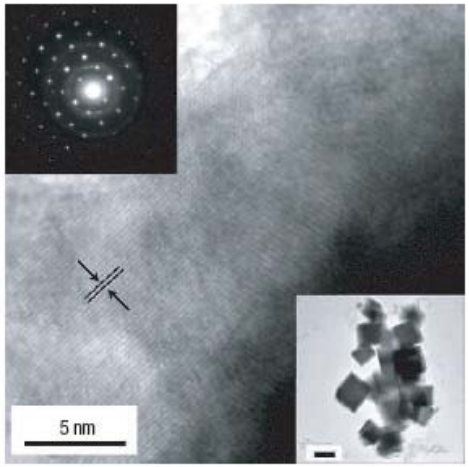

200 nm

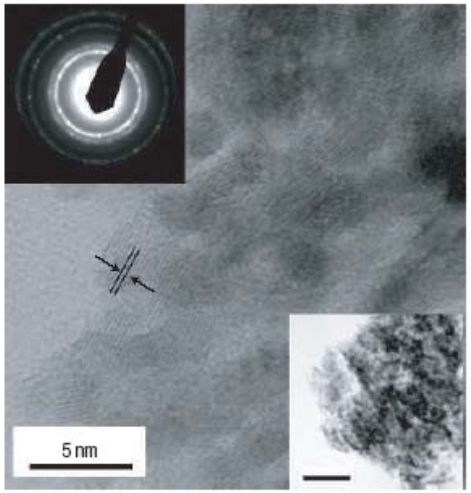

30 nm

Nanoporous Pt

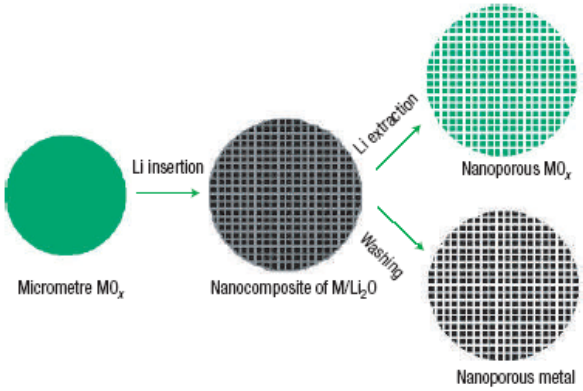

$4Li + RuO_2 \rightarrow Ru{:}2Li_2O$

$Ru{:}2Li_2O \rightarrow RuO_2$ (Nanoporous) + 4Li

$4Li + PtO_2 \rightarrow Pt{:}2Li_2O$

$Pt{:}2Li_2O + 4H^+ \rightarrow Pt$ (Nanoporous) + $4Li^+ + 2H_2O$

Electrochemically synthesized nanoporous Pt showed the enhanced catalytic activities.

Y.-S. Hu and Y.-G. Guo *et al.*
Max-Planck Institute
Nature Mat. (2006).

Nanoporous materials have attracted great technological interest during the past two decades, essentially due to their wide range of applications: they are used as catalysts, molecular sieves, separators and gas sensors as well as for electronic and electrochemical devices[1–5]. Most syntheses of nanoporous materials reported so far have focused on template-assisted bottom-up processes, including soft templating[6–10] (chelating agents, surfactants, block copolymers and so on) and hard templating[11,12] (porous alumina, carbon nanotubes and nanoporous materials) methods. Here, we exploit a mechanism implicitly occurring in lithium batteries at deep discharge[13–18] to develop it into a room-temperature template-free method of wide applicability in the synthesis of not only transition metals but also metal oxides with large surface area and pronounced nanoporosity associated with unprecedented properties. The power of this top-down method is demonstrated by the synthesis of nanoporous Pt and RuO_2, both exhibiting superior performance: the Pt prepared shows outstanding properties when used as an electrocatalyst for methanol oxidation, and the RuO_2, when used as a supercapacitor electrode material, exhibits a distinctly better performance than that previously reported for non-hydrated RuO_2 (refs 19,20).

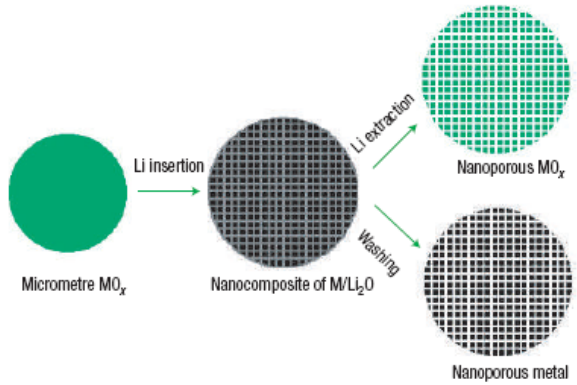

Figure 1 General scheme for the template-free electrochemical lithiation/delithiation synthesis of nanoporous structures.

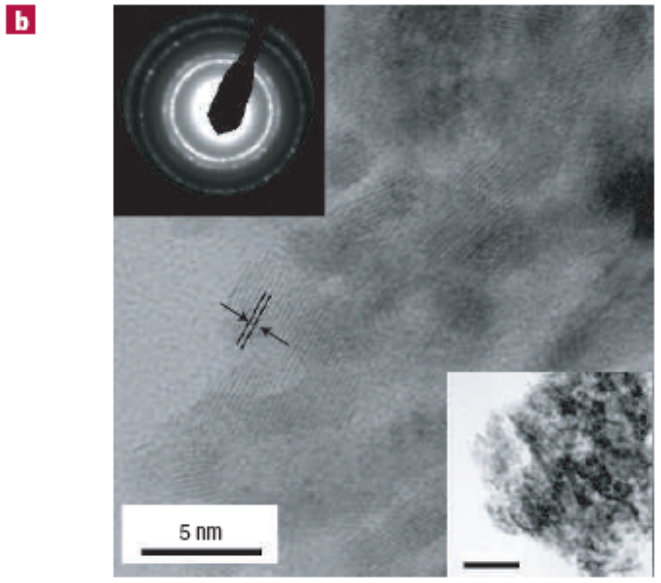

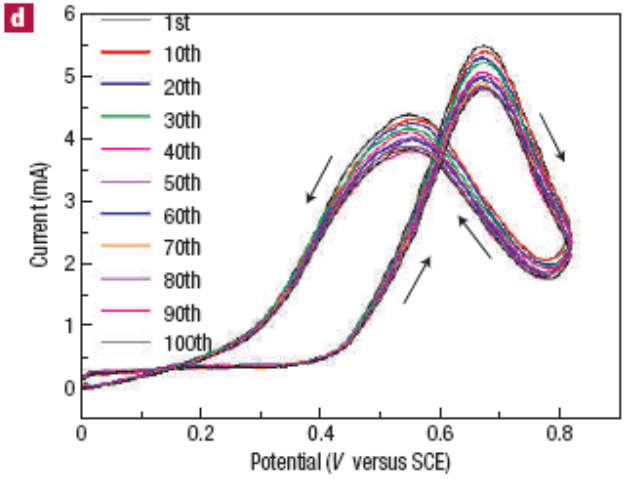

Figure 3 **Characterization of nanoporous Pt. a,b**, HRTEM images of (a) the initial situation—the arrows show the lattice spacing of 0.266 nm, the top left and bottom right insets show the SAED pattern and the overview image of this sample (scale bar, 200 nm); (**b**) discharged to 1.2 V—the arrows show the lattice spacing of 0.226 nm, the top left and bottom right insets show the SAED pattern and the overview image of this sample (scale bar, 30 nm). **c**, Nitrogen adsorption/desorption isotherms of sample (**b**) after washing. Inset: The pore size distribution plot that was calculated by the BJH formula in the adsorption branch isotherm. **d**, Cyclic voltammograms for the nanoporous Pt electrode cycled at a scan rate of 20 mV s^{-1} in 1.0 M methanol in 0.5 M H_2SO_4 solution. The geometric area of the electrode is 0.59 cm^2.

Nanocomposite Materials

- Nanocomposite Materials:
  - Metal nanoparticles + metal-oxide matrix
  - Physical, chemical, and catalytic properties are different from bulk materials.

- Platinum/Metal-Oxide Nanocomposite Catalysts:
  - Pt/WO_3, Pt/RuO_2, etc.
  - Enhanced catalytic activity
    (Physical effects and/or Catalytic effects)

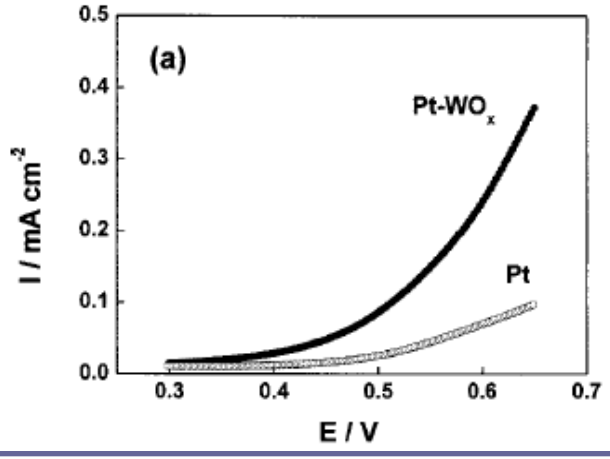

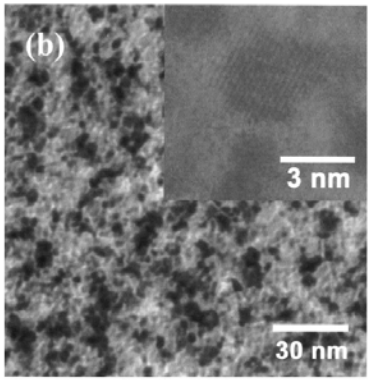

Sung's Group, *SNU*
Appl. Phys. Lett. (2002).

Pt–WO_x electrode structure for thin-film fuel cells

Kyung-Won Park, Kwang-Soon Ahn, Jong-Ho Choi, Yoon-Chae Nah, Young-Min Kim, and Yung-Eun Sung[a)]
Department of Materials Science and Engineering, Kwangju Institute of Science and Technology (K-JIST), Kwangju 500-712, Korea

(Received 1 April 2002; accepted for publication 6 June 2002)

An electrode structure consisting of two phases of Pt and WO_x for use in thin-film fuel cells was designed and fabricated using a cosputtering system with a Pt metal and a tungsten oxide target. The coexistence of a polycrystalline Pt nanosized phase and an amorphous tungsten oxide phase in the electrode layer was confirmed by transmission electron microscopic images and x-ray diffraction data. In addition, compared with a Pt thin-film electrode, the two-phase electrode of Pt and WO_x showed excellent performance for the devices because of the improved activity of the Pt metallic phase and the spill-over effect of porous tungsten oxides. © *2002 American Institute of Physics.*
[DOI: 10.1063/1.1497707]

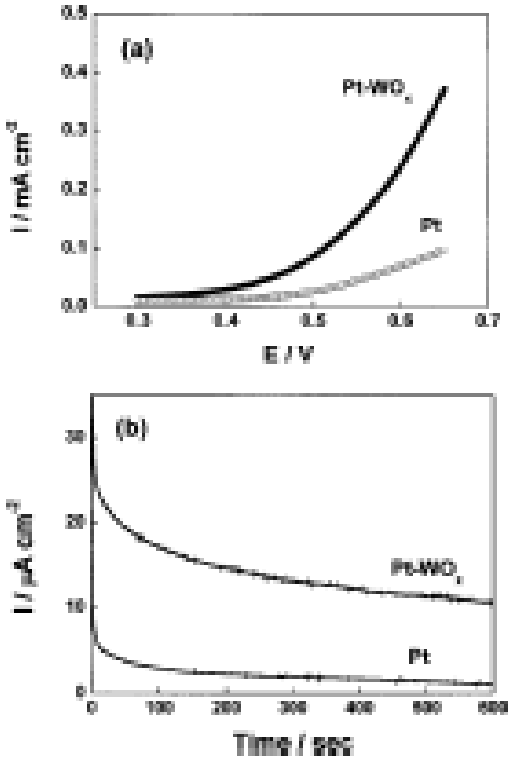

FIG. 3. (a) Current density–accelerating potentials and (b) current density vs time at the oxidation potential for the Pt–WO_x two-phase and the Pt one-phase electrodes.

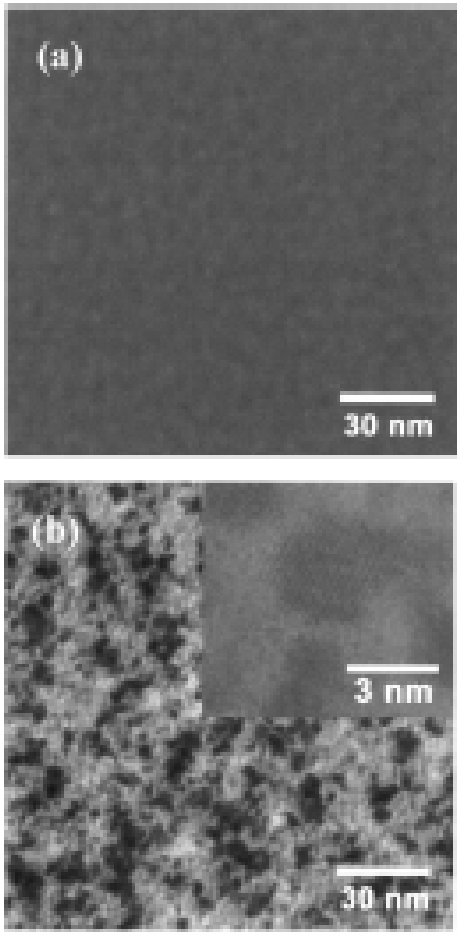

FIG. 1. Transmission electron micrograph of (a) WO_x and (b) Pt–WO_x two-phase electrode deposited using the cosputtering system. The high-resolution TEM image in the inset consists of nanocrystalline Pt and amorphous WO_x in a matrix.

Metal Phosphate

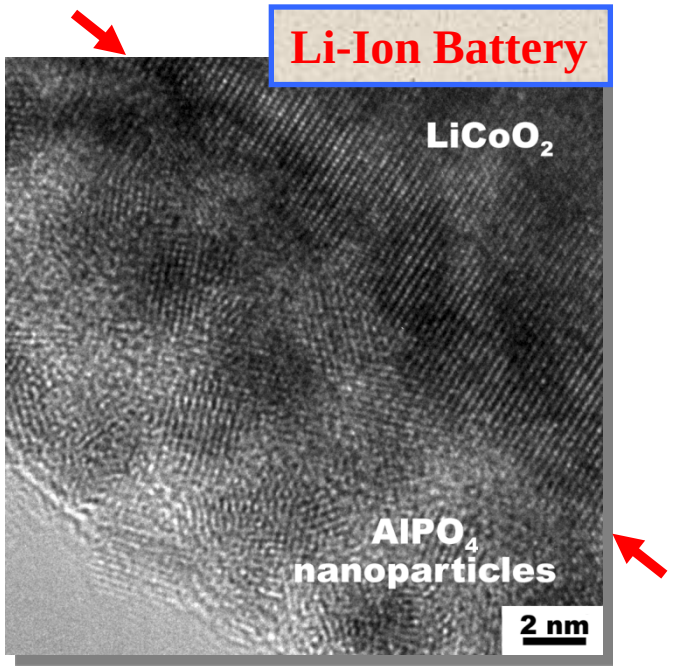

My Group, *Angew. Chem. Int. Ed.* (2003)

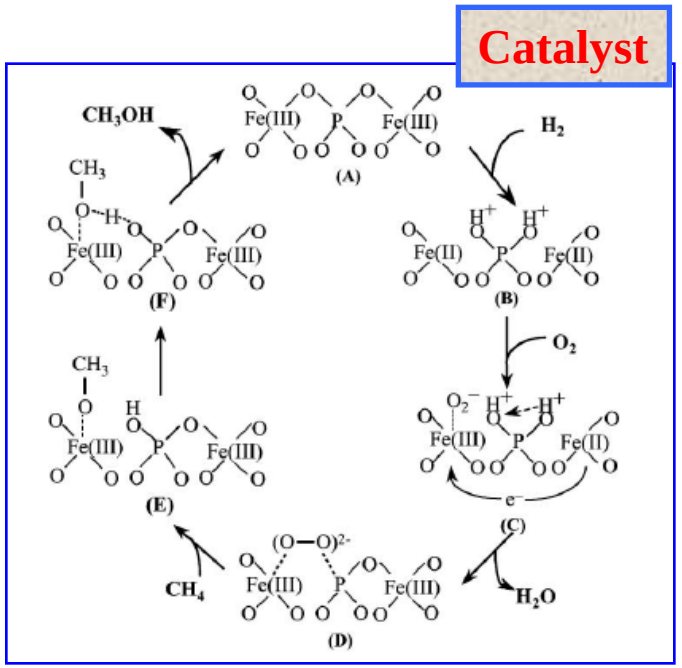

Wang's Group, Tokyo Institute of Technology
J. Catal. (1997).

- **Hydrous $FePO_4$:**
  - **Reasonable Proton Conductivity (~10^{-4} S/cm)**
  - **Good Acidic/Thermal Stability (Anti-Corrosion Additives)**
  - **Partial Oxidation Catalysts (CH_4 → CH_3OH)**
  - **Enhanced CO Oxidation by Bifunctional Mechanisms**

    ($Pt\text{-}CO + M\text{-}OH \rightarrow Pt + M + CO_2 + H^+ + e^-$)

Partial Oxidation of Ethane by Reductively Activated Oxygen over Iron Phosphate Catalyst

Ye Wang and Kiyoshi Otsuka[1]

Department of Chemical Engineering, Tokyo Institute of Technology, Ookayama, Meguro-ku, Tokyo 152, Japan

The catalytic oxidation of ethane was carried out at 573–773 K over iron phosphate catalyst. The oxidation of ethane by oxygen produced only ethylene and carbon oxides. The co-feed of hydrogen with oxygen remarkably accelerated the conversion of ethane. Ethanol and acetaldehyde were newly formed by co-feeding hydrogen. The partial oxidation of ethane to ethanol and acetaldehyde can also be achieved by using nitrous oxide as an oxidant. The co-feed of hydrogen with nitrous oxide increased the conversion of ethane and the yield to C_2 oxygenates. The investigation on the reaction paths suggests that ethanol is the primary product in the oxidation of ethane with hydrogen–oxygen gas mixture and with nitrous oxide. Acetaldehyde and ethylene are produced through further oxidation and dehydration of ethanol, respectively. The highest yield obtained for C_2 oxygenates was 4.4% (ethanol, 1.4%; acetaldehyde, 3.0%) at 673 K. The kinetic and mechanistic studies suggest that the oxidation of ethane proceeds by a similar reaction mechanism to the one proposed for the oxidation of methane. Oxygen is activated by the electrons and protons derived from hydrogen on the catalyst surface, generating a new oxygen species, probably adsorbed peroxide species, effective for the selective oxidation of ethane to ethanol. The same oxygen species can be generated from nitrous oxide by its reductive activation. Both kinetic results and isotopic effects on the conversion of ethane suggest that the dissociation of the C–H bond of ethane proceeds notably faster than the formation of the active oxygen species. In contrast with ethane, the rate of activation of methane was comparable to that of the generation of the active oxygen species.

The oxidation of C_2H_6 must proceed by a similar reaction mechanism on the same active site as shown below.

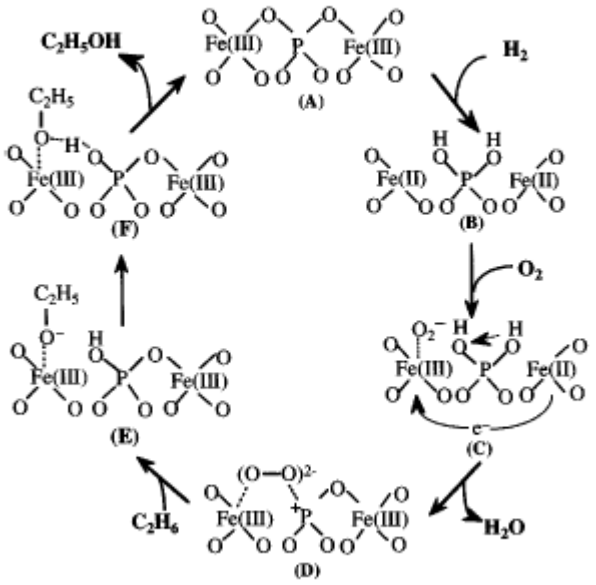

Wang's Group, Tokyo Institute of Technology
J. Catal. (1997).

Journal of The Electrochemical Society, **151** (12) A1989-A1998 (2004)
0013-4651/2004/151(12)/A1989/10/$7.00 © The Electrochemical Society, Inc.

Platinum-Iron Phosphate Electrocatalysts for Oxygen Reduction in PEMFCs

Peter J. Bouwman,[a,b,*] Wojtek Dmowski,[c] Jason Stanley,[a] Gregory B. Cotten,[b] and Karen E. Swider-Lyons[a,*,z]

[a]*Naval Research Laboratory, Surface Chemistry Branch, Washington, DC 20375, USA*
[b]*Department of Chemistry, United States Naval Academy Annapolis, Maryland 21402, USA*
[c]*Department of Materials Science and Engineering, University of Tennessee, Knoxville, Tennessee, USA*

Proton exchange membrane fuel cells (PEMFCs) depend on platinum at the cathode to catalyze the oxygen reduction reaction (ORR) and maintain high performance. This report shows that the electrocatalytic activity of Pt is enhanced when it is dispersed in a matrix of hydrous iron phosphate (FePO). The Pt-FePO has 2 nm micropores with Pt dispersed as ions in Pt^{2+} and Pt^{4+} oxidation states. Increased ORR performance is demonstrated for the Pt-FePO + Vulcan carbon (VC) materials compared to a standard 20 wt % Pt-VC catalyst on rotating disk electrodes with Pt-loadings of 0.1 mg(Pt) cm^{-2}. The improvement in the ORR is attributed to the adsorption/storage of oxygen on the FePO, presumably as iron-hydroperoxides. The ORR activity of the Pt-FePO in air is close to that in oxygen at low current density, and therefore this catalyst has a distinctly unique behavior from Pt-VC. Contrary to Pt-VC, the Pt-FePO catalyst shows activity towards hydrogen and CO oxidation, but does not exhibit their characteristic adsorption peaks, suggesting that Pt ions in the iron phosphate structure are less sensitive to poisoning than metallic Pt. The results present opportunities for new low-Pt catalysts that extend beyond the current capabilities of Pt-VC.
 [DOI: 10.1149/1.1808591]

Manuscript submitted January 30, 2004; revised manuscript received April 5, 2004 Available electronically October 28, 2004.

Pt-Fe-P-O Alloy

K. E. Swider-Lyons' Group, Naval Research Lab.
J. Electrochem. Soc. (2004).

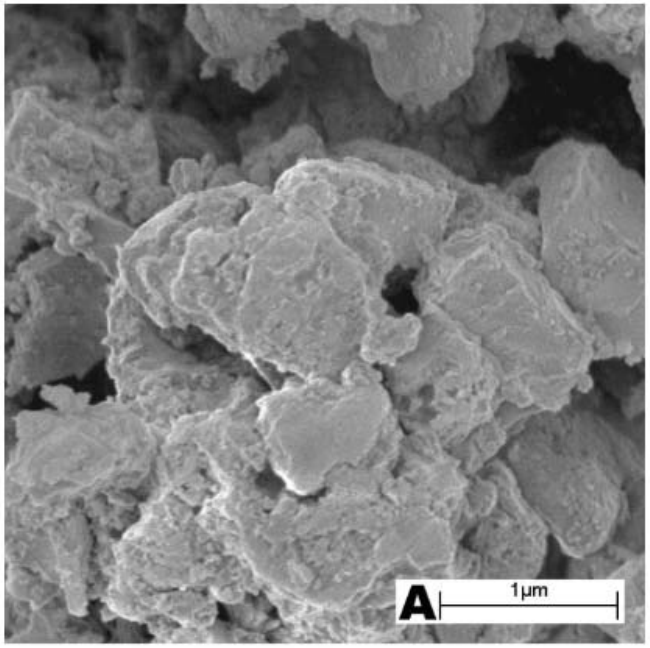

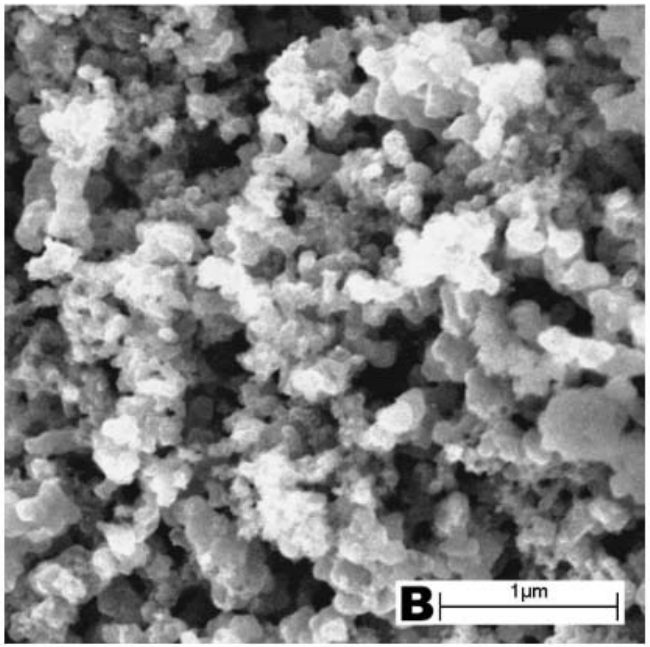

Figure 2. The SEM micrographs show the powder morphology of Pt-FePO (A) and Pt-FePO[*i*VC], (B) after [illegible]

Possible Abilities of $FePO_4$

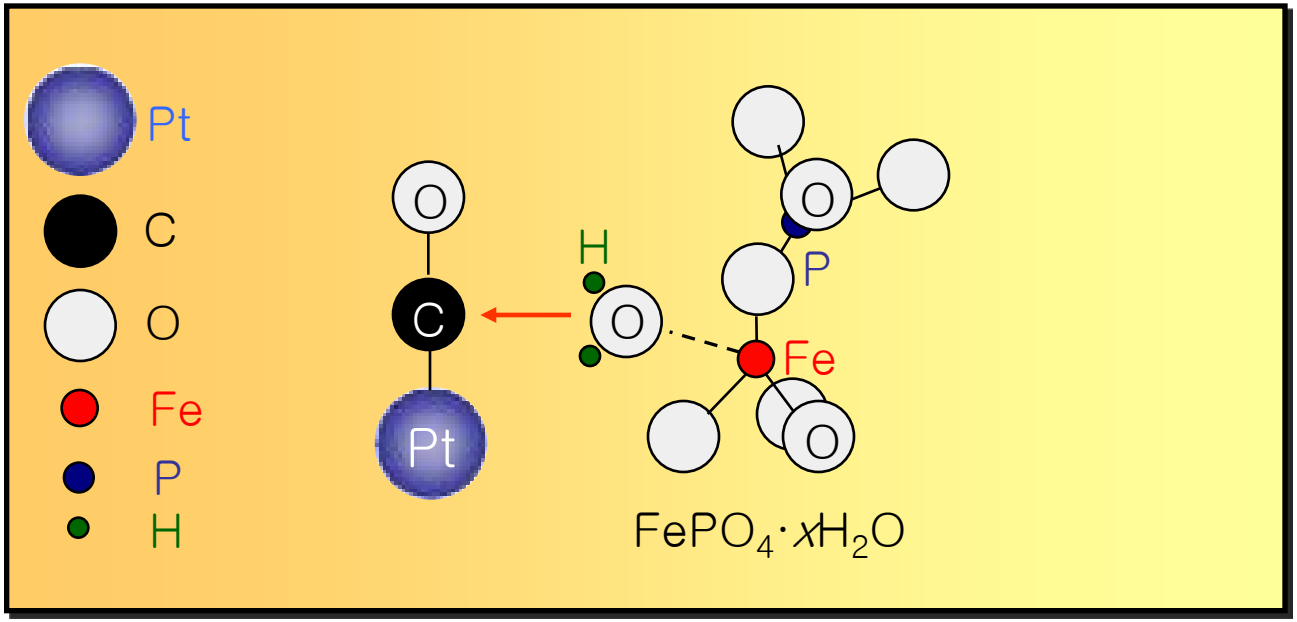

- Hydrous $FePO_4$:
  - Reasonable electron and proton conductivity
  - Enhanced CO oxidation by bifunctional mechanism

  ($Pt\text{-}CO + M\text{-}OH \rightarrow Pt + M + CO_2 + H^+ + e^-$)

Nanostructured Pt-$FePO_4$ Thin-Film Electrode

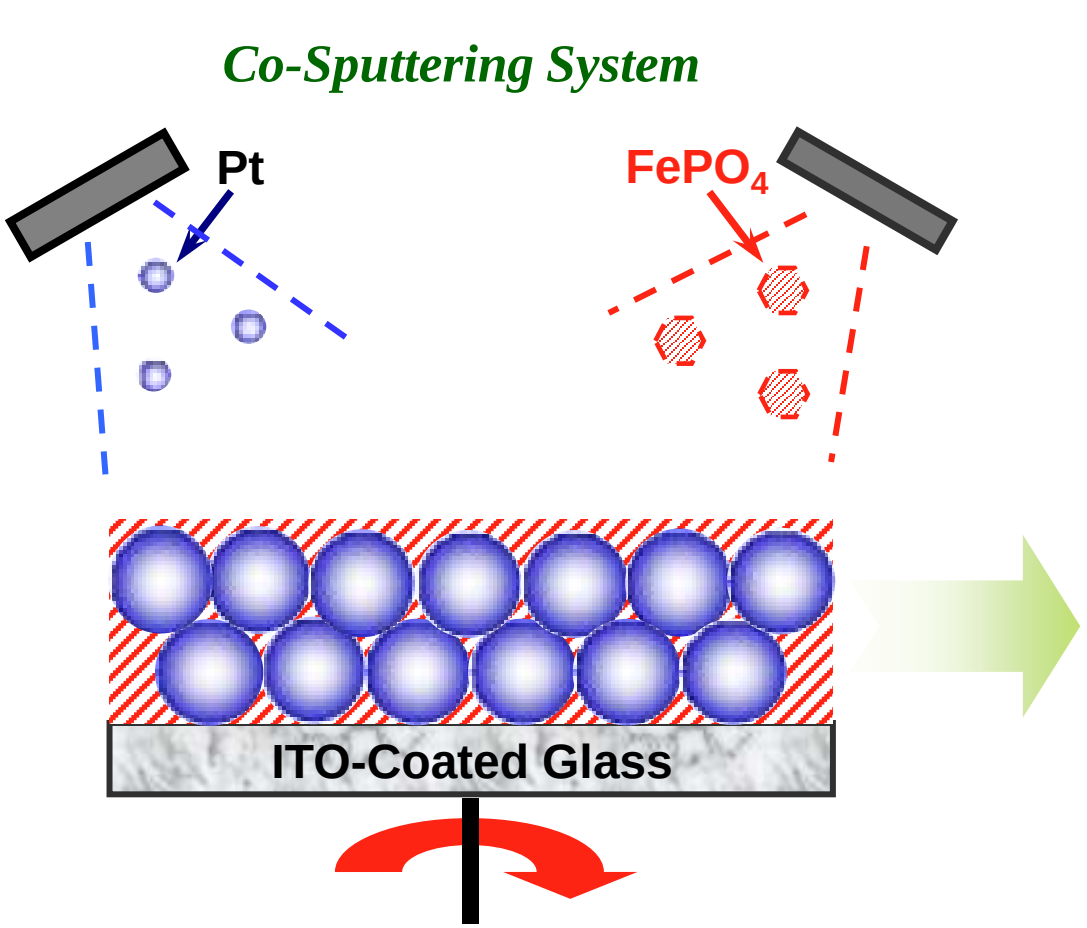

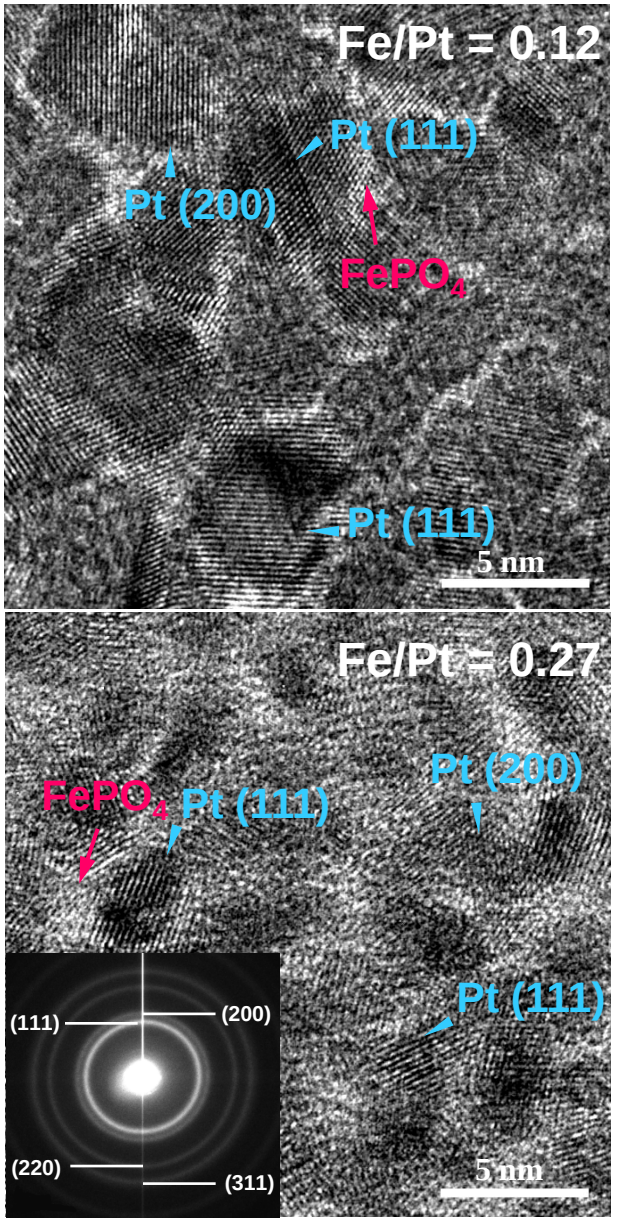

- ❖ Metal/Metal-Phosphate Nanocomposites
- ❖ Control of Nanostructures

➢ B. Lee, C. Kim, Y. Park, T.-G. Kim, and B. Park *Electrochem. Solid-State Lett.* **9**, E27 (2006).

Increased Active Surface Area

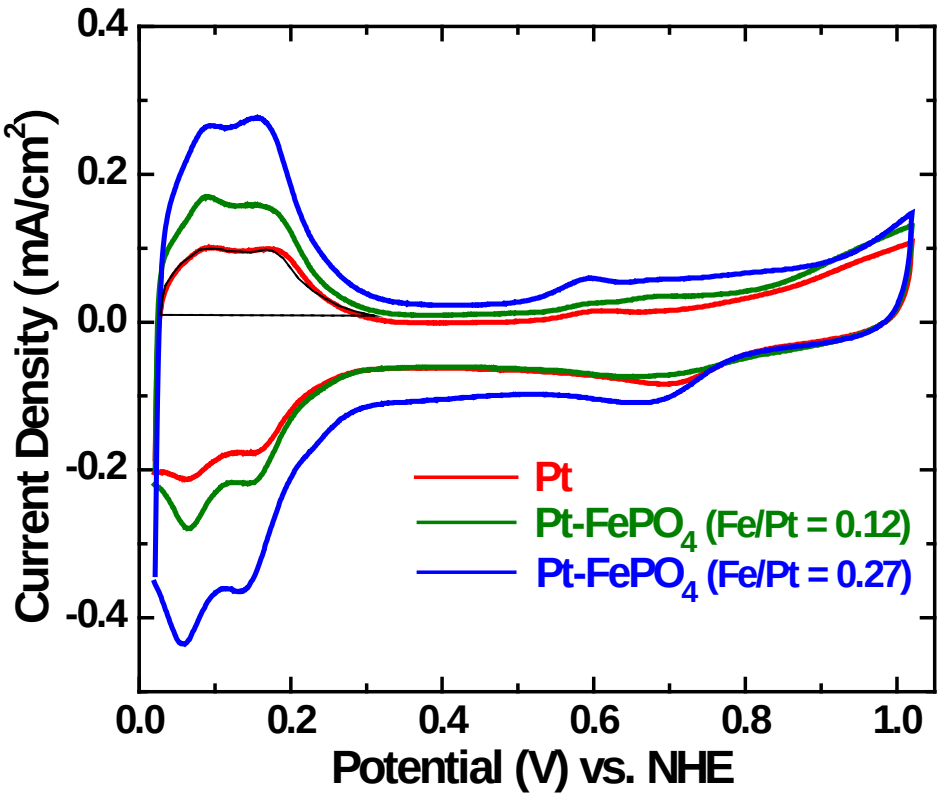

- Shaded Area: Oxidation of hydrogen adsorbed on Pt
- Cyclic voltammetry in 0.5 M H_2SO_4 at 50 mV/s

Enhanced Methanol Oxidation

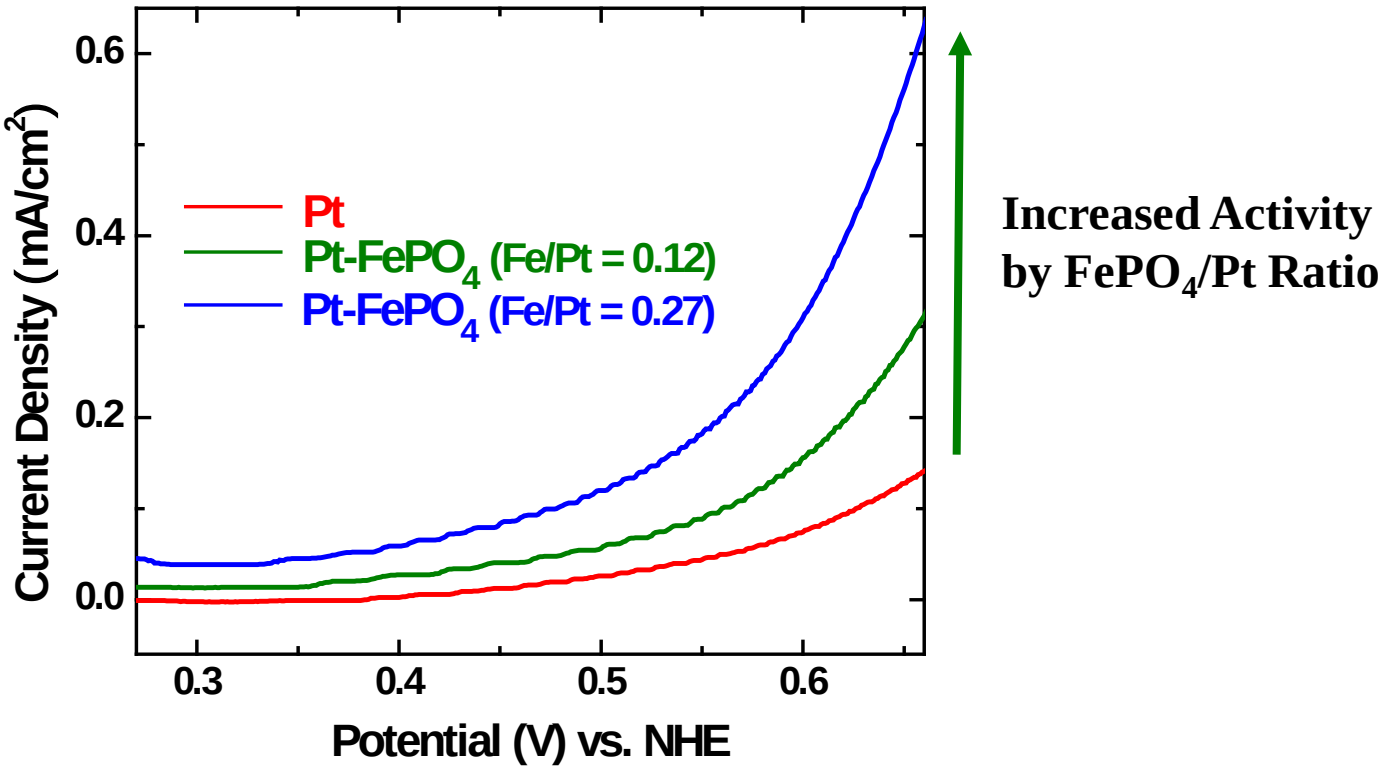

❖ **Pt-FePO$_4$ nanocomposite electrodes:**

- **Higher current density for methanol oxidation**
  - **Increased active surface area of Pt nanophases**
  - **Enhanced activity of Pt by the possible ability of FePO$_4$ matrix**

Steady-State Activities of Nanostructured Thin Films

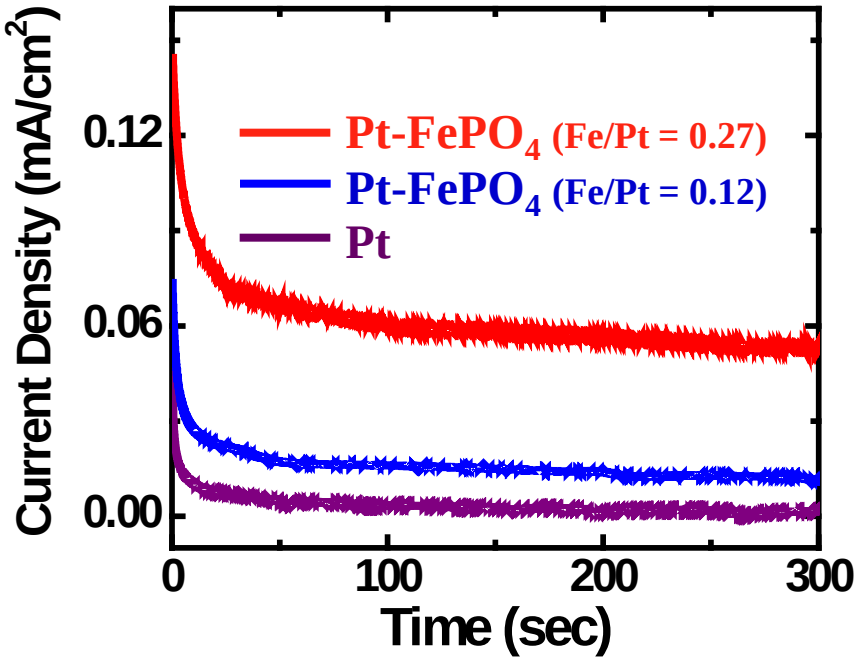

- Pt-$FePO_4$ Nanocomposites:
  - High steady-state activity
  - Low decay rate
- As the atomic ratio (Fe/Pt) increases, the steady-state activity is enhanced.

→
- Effective transfer of protons
- Improved CO oxidation

❖ *Summary*

Electrode	Active surface area	Current density at 0.3 V	Current density at 0.3 V at 300 sec
Pt-$FePO_4$ (Fe/Pt = 0.27)	5.7 cm^2	140 $\mu A/cm^2$	53 $\mu A/cm^2$
Pt-$FePO_4$ (Fe/Pt = 0.12)	3.6 cm^2	70 $\mu A/cm^2$	13 $\mu A/cm^2$
Pt	2.5 cm^2	35 $\mu A/cm^2$	2 $\mu A/cm^2$

Iron Phosphate/Pt Thin-Film Nanostructures

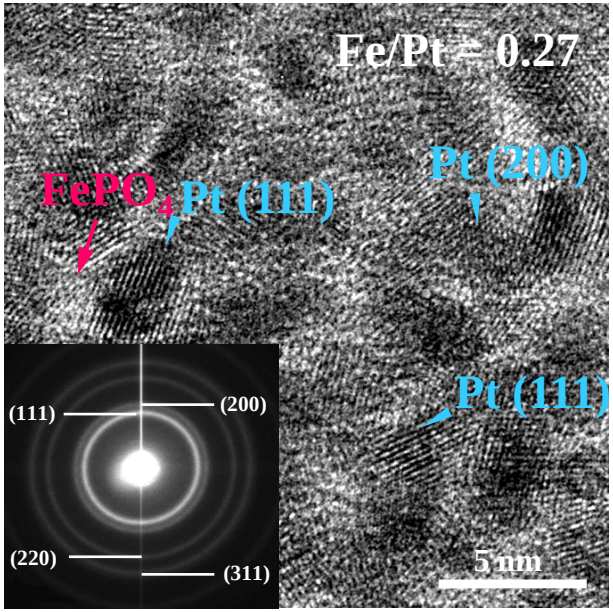

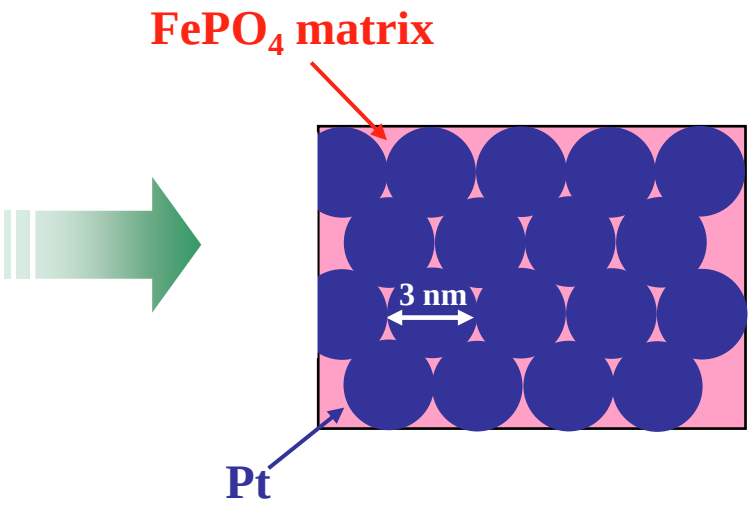

B. Lee, Ph.D. Thesis at SNU (2007)

※ Pt active layer: ~3 layers of Pt nanoparticles

※ Effective thickness of $FePO_4$: ~10 nm

※ Distance between Pt nanoparticles: 1-2 nm

→ $FePO_4$ shows reasonable electron conductivity.

➢ B. Lee, C. Kim, Y. Park, T.-G. Kim, and B. Park *Electrochem. Solid-State Lett.* **9**, E27 (2006).

Suggested Mechanisms of Enhanced CO Oxidation

1. Electronic Effect

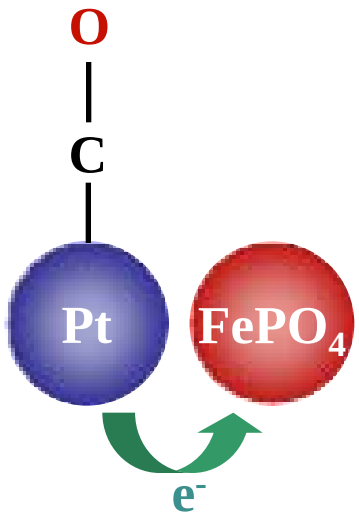

- **Reduction in density of states on the Fermi level**
- **Reduced bonding energy between CO and Pt**

Goodenough's Group, *Univ. of Texas at Austin*, *Chem. Mater.* (1989).
Wiekowski's Group, *UIUC*, *J. Phys. Chem.* (1994).

2. Bifunctional Effect

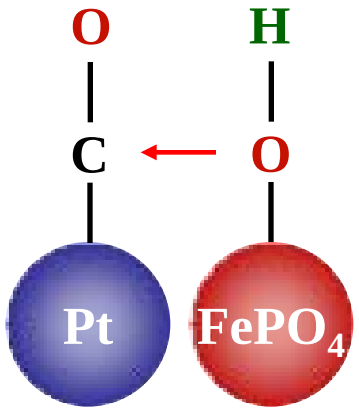

- **Metal phosphate provides "active" OH.**
- **$Pt\text{-}CO + FePO_4\text{-}OH \rightarrow Pt + FePO_4 + CO_2 + H^+ + e^-$**

Watanabe's Group, *Yamanashi Univ.*, *J. Electroanal. Chem.* (1975).
Cairns's Group, *Lawrence Berkeley Lab.*, *J. Phys. Chem.* (1993).

Current Issues in Pt Catalysts

- ❖ Poor Stability during Long-Term Operation
- ❖ Slow Oxygen-Reduction Kinetics
- ❖ Easy Poisoning by Pollutants
- ❖ High Cost

Nanostructured Catalysts

- Nanocomposites
- Nanoporous Materials

Instabilities of Fuel Cells during Long-Term Operation

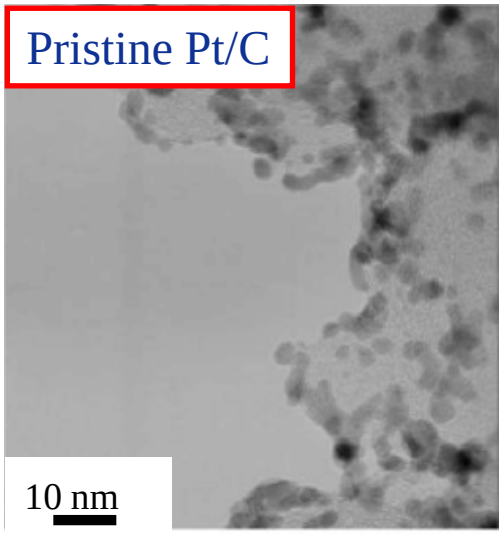

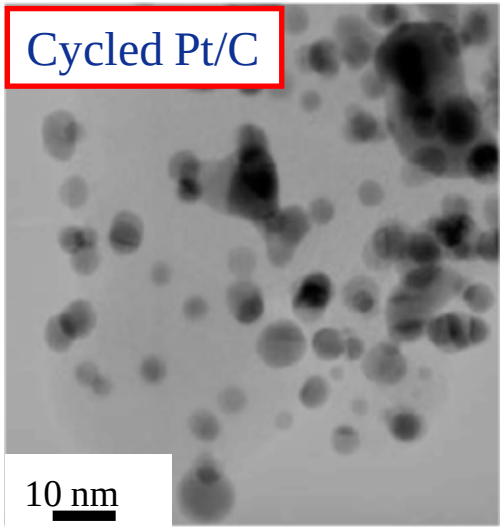

Figure 8. Typical TEM micrographs from (a) the pristine Pt/Vulcan samples powder sample and (b) powders scraped away from the cathode surface of the cycled MEA sample. Considerable coarsening of spherically shaped platinum nanoparticles was found after potential cycling.

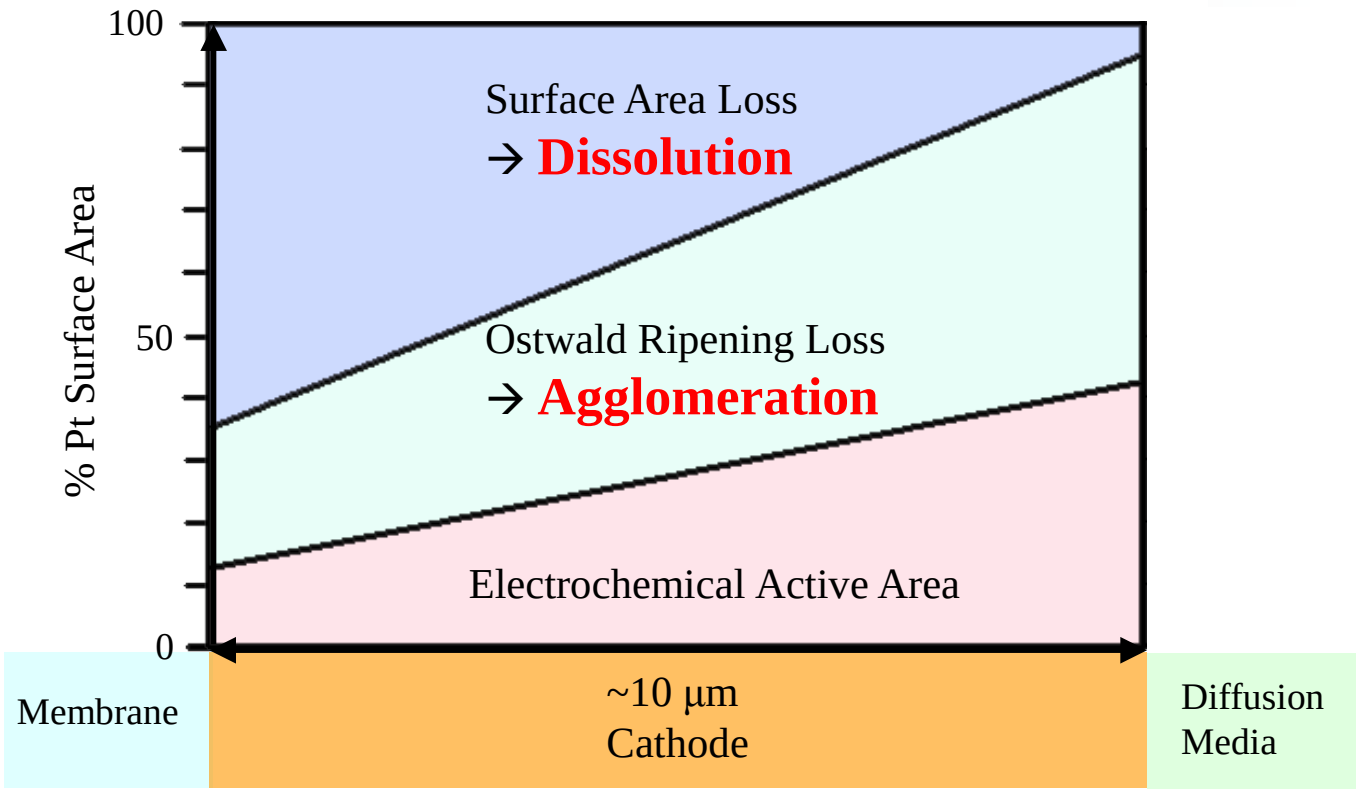

- The Significant Electrochemical Active Area Loss:
  Agglomeration and Dissolution of Pt Nanoparticles

"Instability of Pt/C Electrocatalysts in PEMFC"
Y. Shao-Horn's Group (MIT), *J. Electrochem. Soc.* (2005).

Instability of Pt/C Electrocatalysts in Proton Exchange Membrane Fuel Cells

A Mechanistic Investigation

P. J. Ferreira,[a,d] G. J. la O',[a,*] Y. Shao-Horn,[a,**,z] D. Morgan,[b] R. Makharia,[c] S. Kocha,[c,**] and H. A. Gasteiger[c,**]

[a]*Massachusetts Institute of Technology, Cambridge, Massachusetts 02139, USA*
[b]*University of Wisconsin–Madison, Madison, Wisconsin 53706, USA*
[c]*General Motors Fuel Cell Activities, Honeoye Falls, New York 14472, USA*

Equilibrium concentrations of dissolved platinum species from a Pt/C electrocatalyst sample in 0.5 M H_2SO_4 at 80°C were found to increase with applied potential from 0.9 to 1.1 V vs reversible hydrogen electrode. In addition, platinum surface area loss for a short-stack of proton exchange membrane fuel cells (PEMFCs) operated at open-circuit voltage (~0.95 V) was shown to be higher than another operated under load (~0.75 V). Both findings suggest that the formation of soluble platinum species (such as Pt^{2+}) plays an important role in platinum surface loss in PEMFC electrodes. As accelerated platinum surface area loss in the cathode (from 63 to 23 m^2/g_{Pt} in ~100 h) was observed upon potential cycling, a cycled membrane electrode assembly (MEA) cathode was examined in detail by incidence angle X-ray diffraction and transmission electron microscopy (TEM) to reveal processes responsible for observed platinum loss. In this study, TEM data and analyses of Pt/C catalyst and cross-sectional MEA cathode samples unambiguously confirmed that coarsening of platinum particles occurred via two different processes: (*i*) Ostwald ripening on carbon at the nanometer scale, which is responsible for platinum particle coarsening from ~3 to ~6 nm on carbon, and (*ii*) migration of soluble platinum species in the ionomer phase at the micrometer scale, chemical reduction of these species by crossover H_2 molecules, and precipitation of platinum particles in the cathode ionomer phase, which reduces the weight of platinum on carbon. It was estimated that each process contributed to ~50% of the overall platinum area loss of the potential cycled electrode.
 [DOI: 10.1149/1.2050347]

Manuscript submitted May 10, 2005; revised manuscript received June 24, 2005. Available electronically October 7, 2005.

Instability of Pt Catalysts

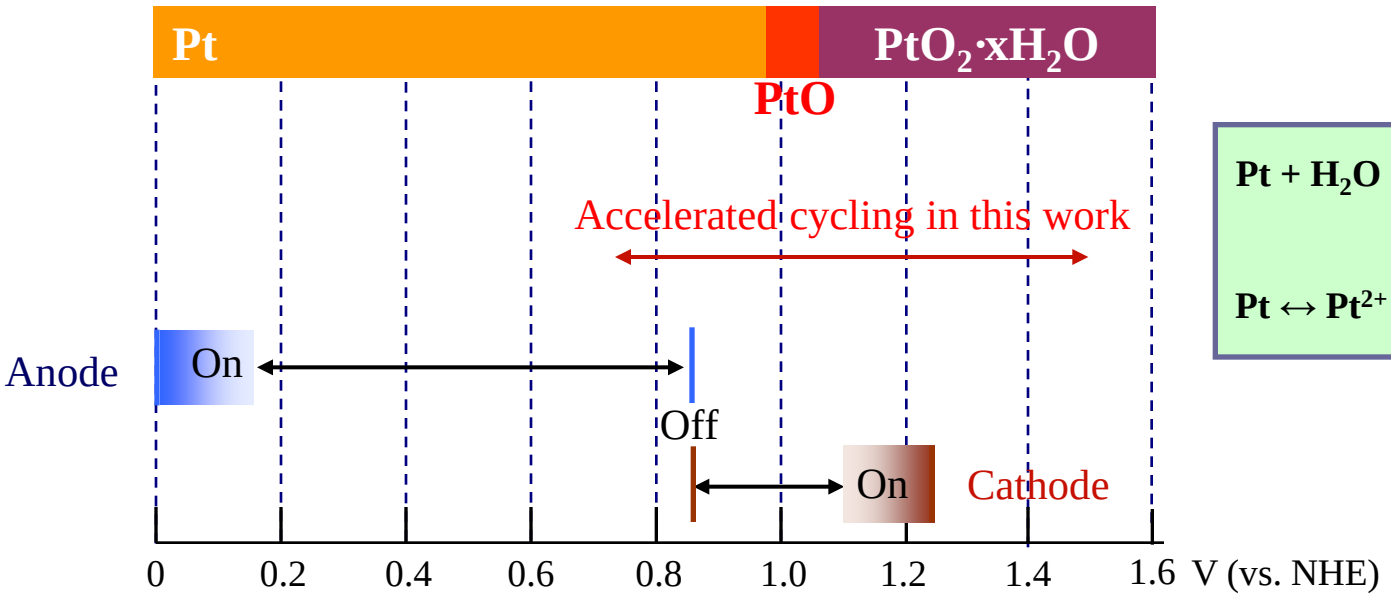

$Pt + H_2O \leftrightarrow PtO + 2H^+ + 2e^-$ $E = 0.98$ V

$Pt \leftrightarrow Pt^{2+} + 2e^-$ $E = 1.18$ V

- Pt Dissolution at the Cathode
  - Stable at a Wide Potential Range
  - Abrupt Potential Change at the On/Off Operation → Dissolution of Pt

  "Mathematical Model of Platinum Movement in PEM Fuel Cells"

  UTC Fuel Cells, *J. Electrochem. Soc.* (2003)

- Pt dissolution in this work was accelerated with the repeated cycling.

  (0.68 – 1.48 V, 500 mV/s for 1000 cycles)

Synthesis of $FePO_4$-Pt/C Nanocomposites

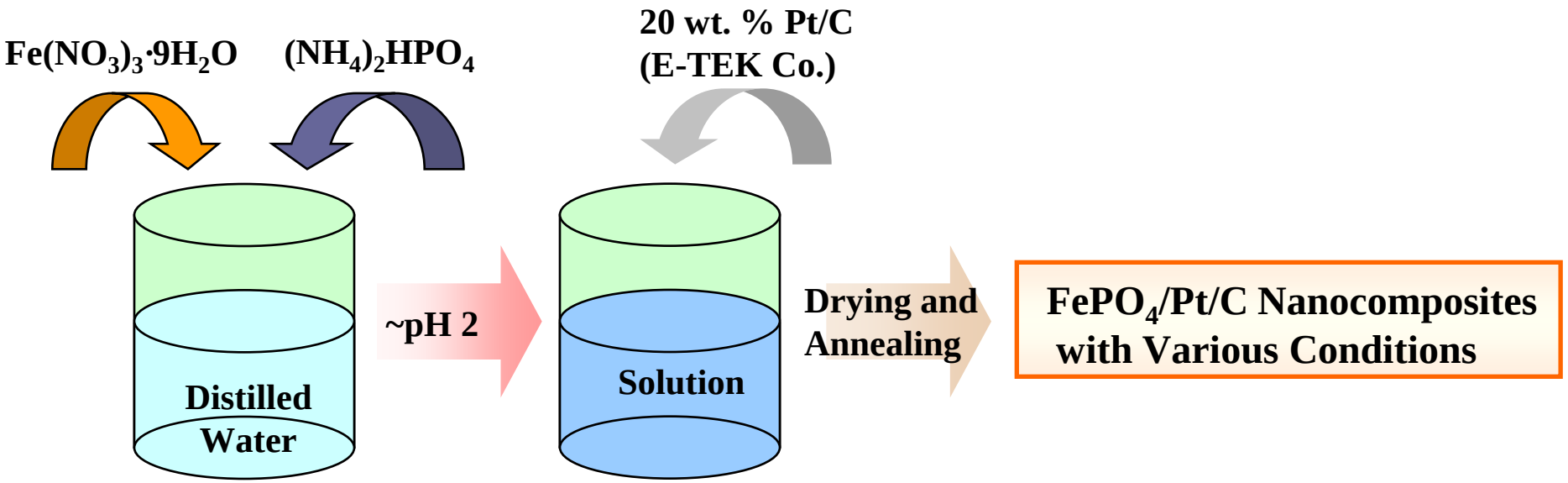

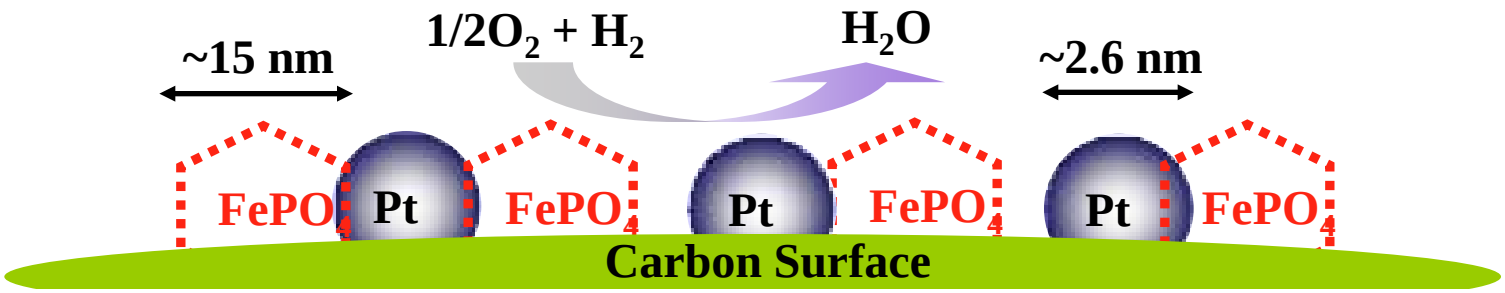

Nanostructures of $FePO_4$/Pt/C Nanocomposites

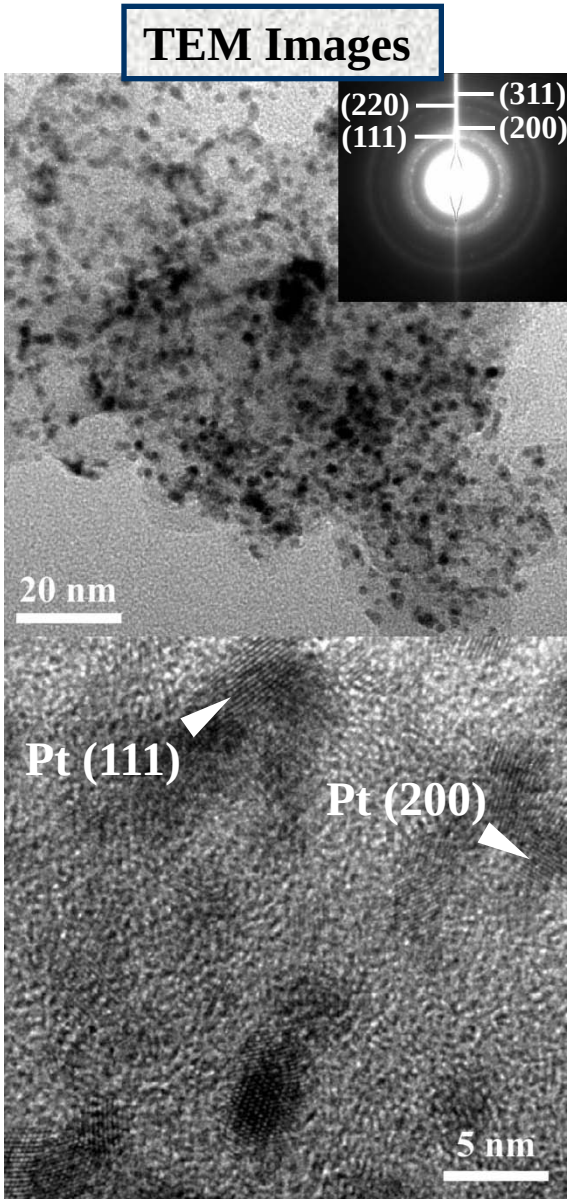

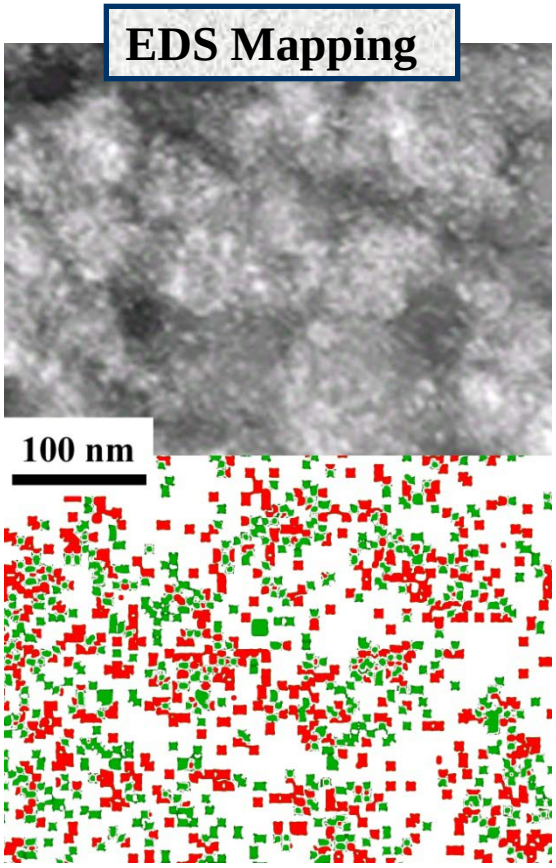

$FePO_4$ and Pt nanoparticles are well dispersed.

➢ C. Kim, B. Lee, Y. Park, J. Lee, H. Kim, and B. Park *Appl. Phys. Lett.* **91**, 113101 (2007).

XPS of $FePO_4$-Pt/C Nanocomposites

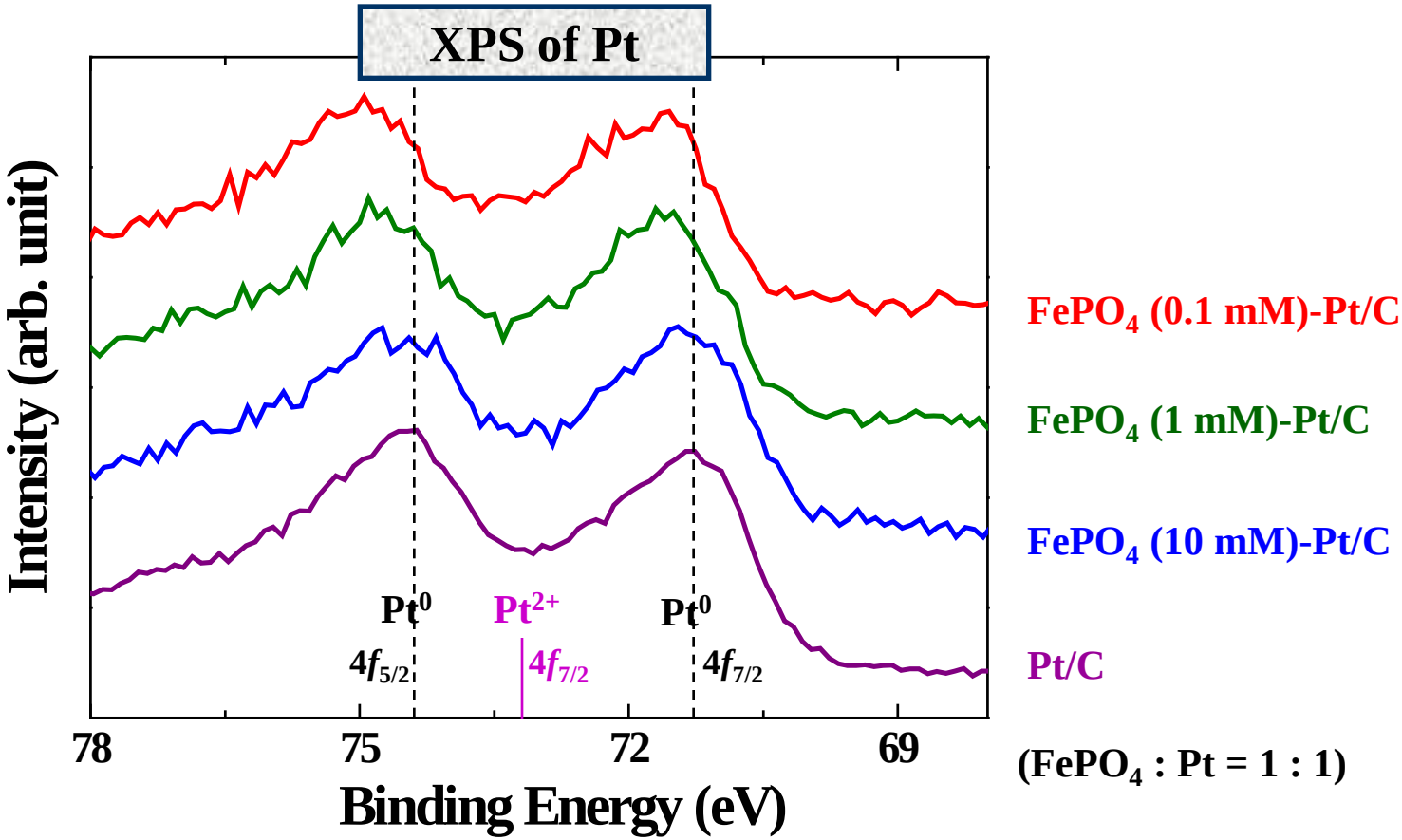

Slight Peak Shift of Pt in $FePO_4$-Pt/C Nanocomposites

- **Zero-Valent Metallic Pt Phase**
- **Charge Transfer of Pt**
- **The Largest Interfacial Contacts in $FePO_4$ (0.1 mM)-Pt/C**

Electrocatalytic Properties of $FePO_4$/Pt/C Nanocomposites

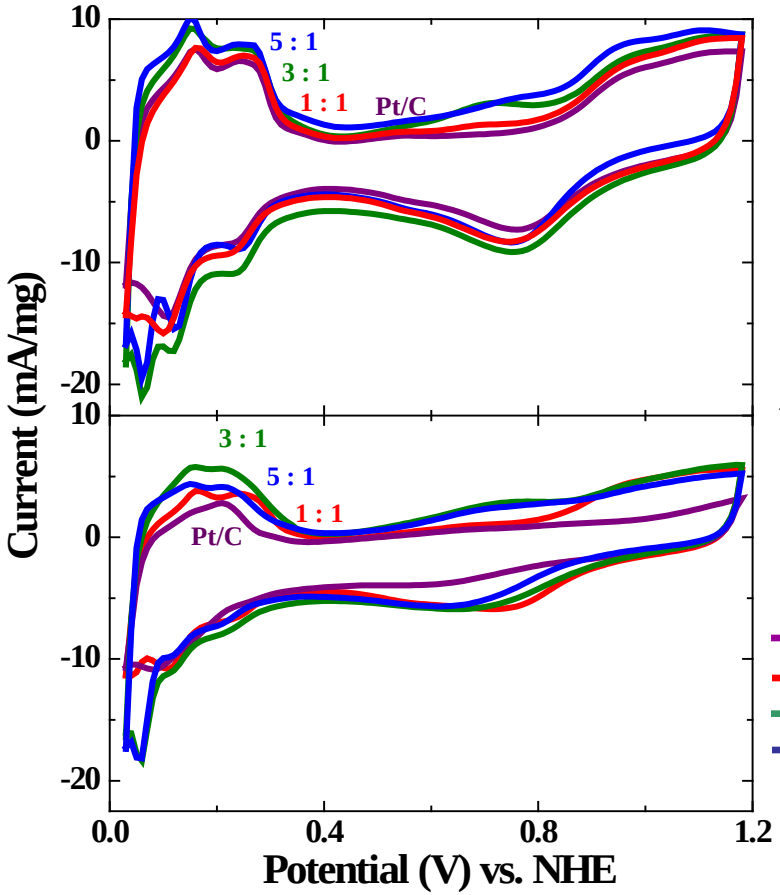

After 1000 Cycles

Pt/C
$FePO_4$: Pt/C = 1 : 1
$FePO_4$: Pt/C = 3 : 1
$FePO_4$: Pt/C = 5 : 1
($FePO_4$ 0.1 mM)

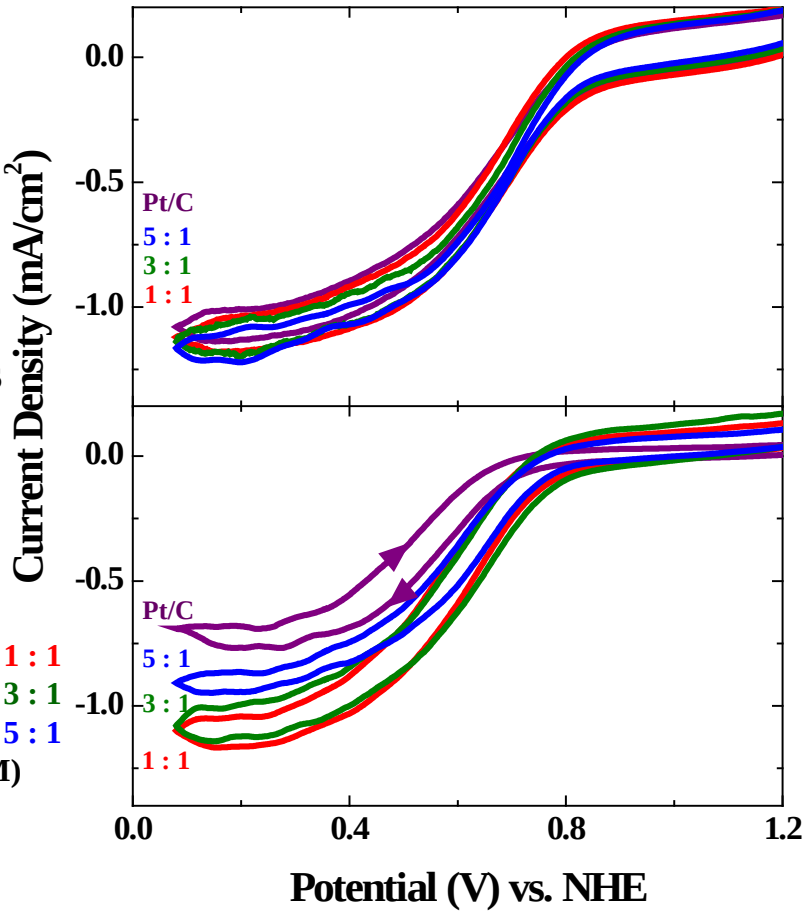

$FePO_4$/Pt ratio of 1 and 3 showed the best enhanced long-term stabilities.

- **The Decreased Loss of Electrochemical Active Area**
- **More Conserved Oxygen-Reduction Reaction**

Agglomeration after 1000 Cycles

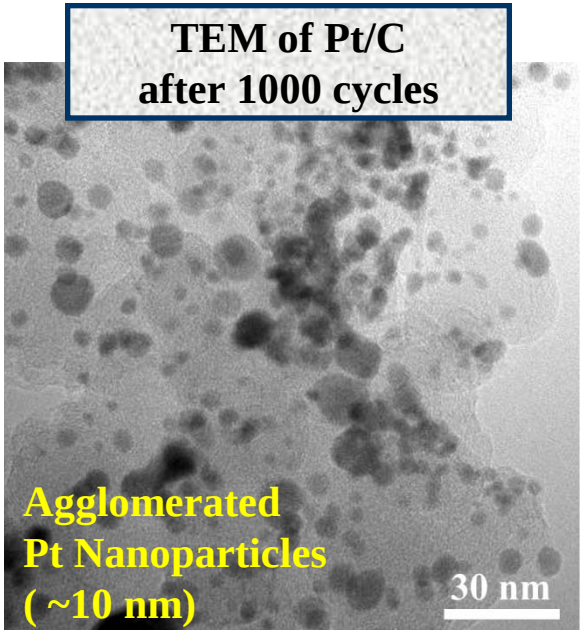

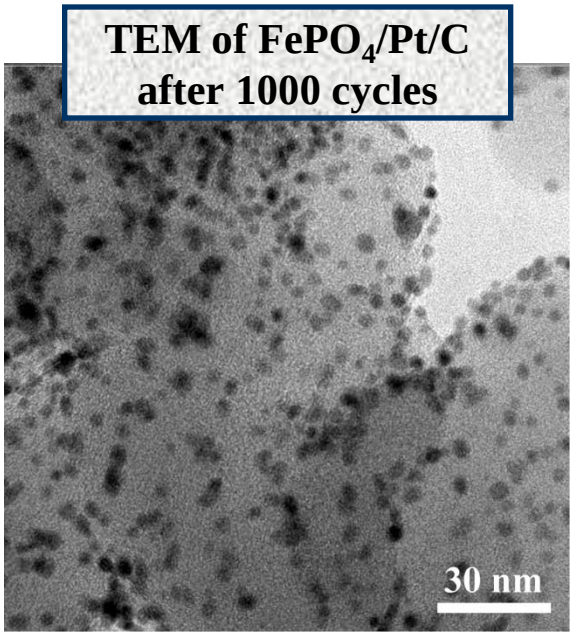

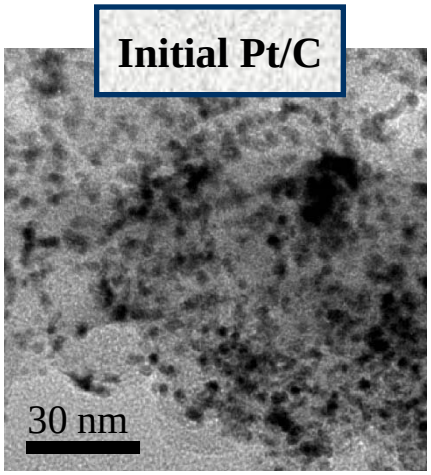

Similar Nanoparticle Size to the Initial Stage

Synthetic Concentration of $FePO_4$	Molar Ratio ($FePO_4$: Pt)	Electrochemical Surface Area[1]	Dissolution of Pt (at. %)[2]
Pt/C	0 : 1	41%	18%
$FePO_4$ (0.1 mM)/Pt/C	1 : 1	53%	4%
	3 : 1	71%	3%
	5 : 1	50%	11%
$FePO_4$ (1 mM)/Pt/C	1 : 1	47%	6%
$FePO_4$ (10 mM)/Pt/C	1 : 1	46%	14%

[1] ESA: Measured by Hydrogen Desorption (from initial 100%)

[2] Dissolution into Electrolyte (by ICP)

Suggested Mechanisms for Enhanced Stability I

1. Stabilization of Pt by the modification of the electronic structures due to the charge transfer with $FePO_4$.

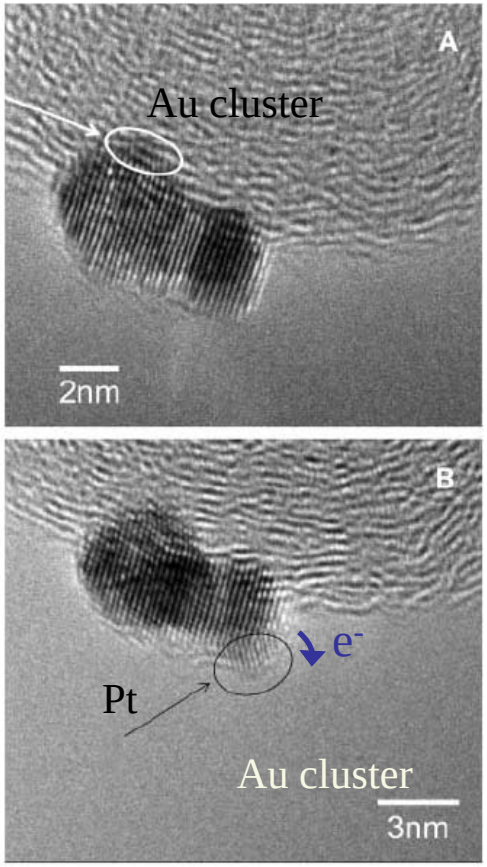

Fig. 2. Electron micrographs of a Au/Pt/C catalyst made by displacement of a Cu monolayer by Au. High-resolution images (**A** and **B**) show atomic rows with spacings that are consistent with the Pt(111) single-crystal structure. A different structure in the areas indicated by the arrows is ascribed to the Au clusters.

Electron-poor Pt nanoparticles by Au clusters exhibited the enhanced stabilities.

"Stabilization of Platinum Oxygen-Reduction Electrocatalysts Using Gold Clusters"
R. R. Adzic's Group, *Science* (2007).

Stabilization of Platinum Oxygen-Reduction Electrocatalysts Using Gold Clusters

J. Zhang,[1] K. Sasaki,[1] E. Sutter,[2] R. R. Adzic[1]

We demonstrated that platinum (Pt) oxygen-reduction fuel-cell electrocatalysts can be stabilized against dissolution under potential cycling regimes (a continuing problem in vehicle applications) by modifying Pt nanoparticles with gold (Au) clusters. This behavior was observed under the oxidizing conditions of the O_2 reduction reaction and potential cycling between 0.6 and 1.1 volts in over 30,000 cycles. There were insignificant changes in the activity and surface area of Au-modified Pt over the course of cycling, in contrast to sizable losses observed with the pure Pt catalyst under the same conditions. In situ x-ray absorption near-edge spectroscopy and voltammetry data suggest that the Au clusters confer stability by raising the Pt oxidation potential.

Suggested Mechanisms for Enhanced Stability I

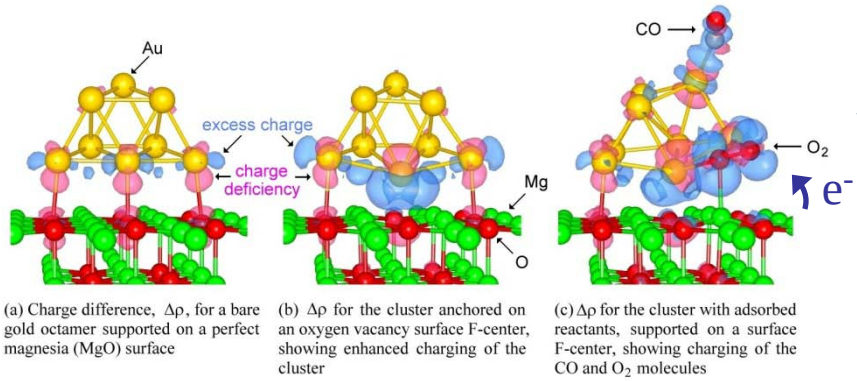

(a) Charge difference, $\Delta\rho$, for a bare gold octamer supported on a perfect magnesia (MgO) surface (b) $\Delta\rho$ for the cluster anchored on an oxygen vacancy surface F-center, showing enhanced charging of the cluster (c) $\Delta\rho$ for the cluster with adsorbed reactants, supported on a surface F-center, showing charging of the CO and O_2 molecules

Electron-rich Au clusters showed the enhanced catalytic properties.

"Charging Effects on Bonding and Catalyzed Oxidation of CO on Au_8 Clusters on MgO"
U. Landman's Group, *Science* (2005).

Charging Effects on Bonding and Catalyzed Oxidation of CO on Au_8 Clusters on MgO

Bokwon Yoon,[1] Hannu Häkkinen,[1]* Uzi Landman,[1]† Anke S. Wörz,[2] Jean-Marie Antonietti,[2] Stéphane Abbet,[2] Ken Judai,[2] Ueli Heiz[2]†

Gold octamers (Au_8) bound to oxygen-vacancy F-center defects on Mg(001) are the smallest clusters to catalyze the low-temperature oxidation of CO to CO_2, whereas clusters deposited on close-to-perfect magnesia surfaces remain chemically inert. Charging of the supported clusters plays a key role in promoting their chemical activity. Infrared measurements of the stretch vibration of CO adsorbed on mass-selected gold octamers soft-landed on MgO(001) with coadsorbed O_2 show a red shift on an F-center–rich surface with respect to the perfect surface. The experiments agree with quantum ab initio calculations that predict that a red shift of the C–O vibration should arise via electron back-donation to the CO antibonding orbital.

Suggested Mechanisms for Enhanced Stability II

2. $FePO_4$ nanoparticles can passivate the active paths for the agglomeration of Pt nanoparticles.

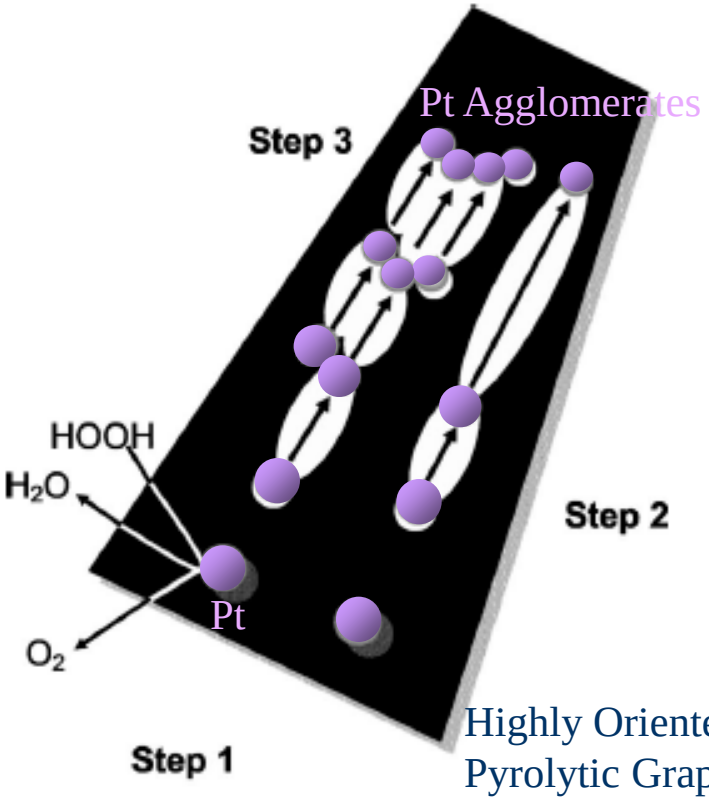

Pt nanoparticles can migrate easily through etched carbon surface and agglomerate into larger Pt.

"Stability of Pt-Catalyzed Highly Oriented Pyrolytic Graphite Against Hydrogen Peroxide in Acid Solution"
Z. Ogumi's Group, *J. Electrochem Soc.* (2006).

Stability of Pt-Catalyzed Highly Oriented Pyrolytic Graphite Against Hydrogen Peroxide in Acid Solution

Taro Kinumoto,[a] Kenji Takai,[a] Yasutoshi Iriyama,[a] Takeshi Abe,[a,*] Minoru Inaba,[b,*] and Zempachi Ogumi[a,**,z]

[a]*Department of Energy and Hydrocarbon Chemistry, Graduate School of Engineering, Kyoto University, Nishikyo-ku, Kyoto 615-8510, Japan*
[b]*Department of Molecular Science and Technology, Faculty of Engineering, Doshisha University, Kyotanabe, Kyoto 610-0321, Japan*

Aiming at clarifying the effects of hydrogen peroxide on the degradation of Pt/C catalyst in polymer electrolyte fuel cells (PEFCs), a model electrode for the Pt/C catalyst was prepared by electrodeposition of Pt on highly oriented pyrolytic graphite (HOPG) and its durability against hydrogen peroxide investigated. After storage in acidic 1.0 mol dm^{-3} H_2O_2 solution at room temperature, many scars were formed by oxidative etching of HOPG and Pt-particle catalysts aggregated on the surface. In contrast, no surface change was observed without hydrogen peroxide. These results showed that hydrogen peroxide significantly deteriorates the Pt/HOPG electrode, and the active surface area of the Pt particles, which was determined by cyclic voltammetry, was reduced after immersion in the H_2O_2 solution. The influence of applied potential was also investigated, and the deterioration of the electrode was accelerated at potentials both more positive and negative than open-circuit potential (ca. 0.8 V). Moreover, similar degradation phenomenon was observed when the potential was set at 0.1 V, at which a large amount of H_2O_2 is formed in oxygen reduction, in O_2-saturated H_2O_2-free acid solution for 5 days.
 [DOI: 10.1149/1.2130665]

Manuscript submitted June 15, 2005; revised manuscript received August 30, 2005. Available electronically November 28, 2005.

"Stability of Pt-Catalyzed Highly Oriented Pyrolytic Graphite Against Hydrogen Peroxide in Acid Solution"
Z. Ogumi's Group, *J. Electrochem Soc.* (2006).

Motivation: Problems of Ru Crossover

- Degradation of electrode performance by long-term operations:
  - Dissolution of noble metal-based catalysts
  - Agglomeration of catalyst nanoparticles

- For PtRu catalyst in DMFC Anode:
  - Ru Crossover from PtRu Anode to Pt Cathode

  [Zeleney's Group, *Los Alamos National Lab.*, *J. Electrochem. Soc.* (2004)]

- Impacts of Ru Dissolution:
  - Methanol Oxidation ↓
  - Membrane Performance ↓
  - Oxygen Reduction ↓

➡ ***Need to Block Ru Crossover***

Motivation: Ru Oxidation Potential and DMFC Operating Potential

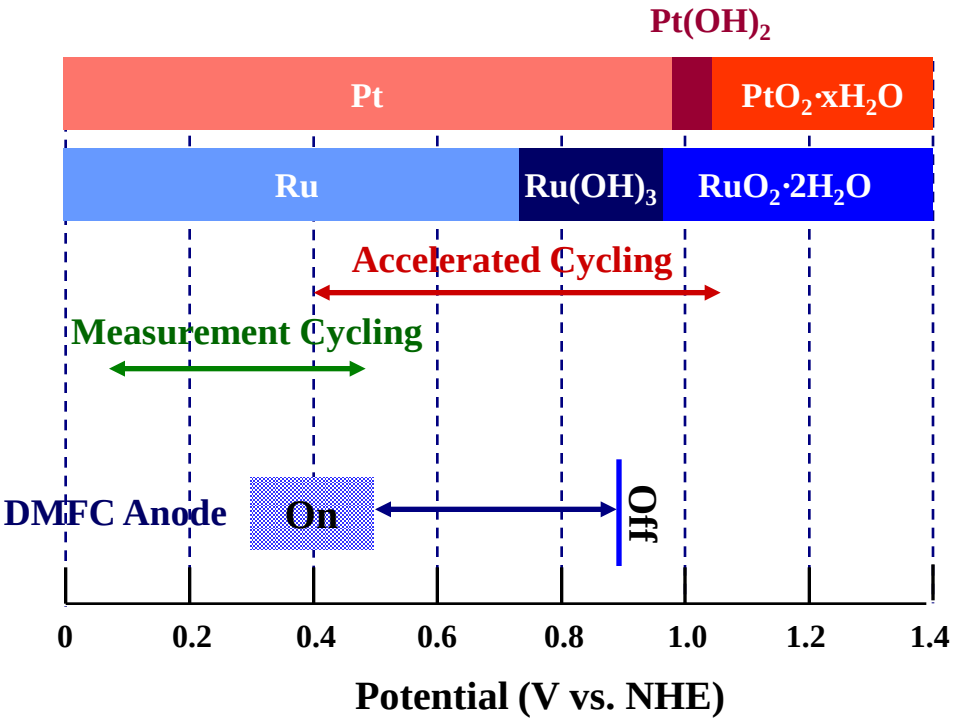

$Ru + 3H_2O \leftrightarrow Ru(OH)_3 + 3H^+ + 3e^-$

$E = 0.738$ V

$Pt + 2H_2O \leftrightarrow Pt(OH)_2 + 2H^+ + 2e^-$

$E = 0.980$ V

$Ru \leftrightarrow Ru^{2+} + 2e^-$

$E = 0.455$ V

- Ru dissolution of PtRu:
  - Abrupt high potential is applied to DMFC anode when fuel cell is turned off.
    [duPont Inc., *J. Phys. Chem. B* (2004)]
- Investigation of Ru dissolution in this work
  with the accelerated potential cycling (200 cycles, 0.4 – 1.05 V)

➡ ***Ru^+ can be reduced within the DMFC operating-potential ranges.***

Motivation: Metal-Phosphate Coating

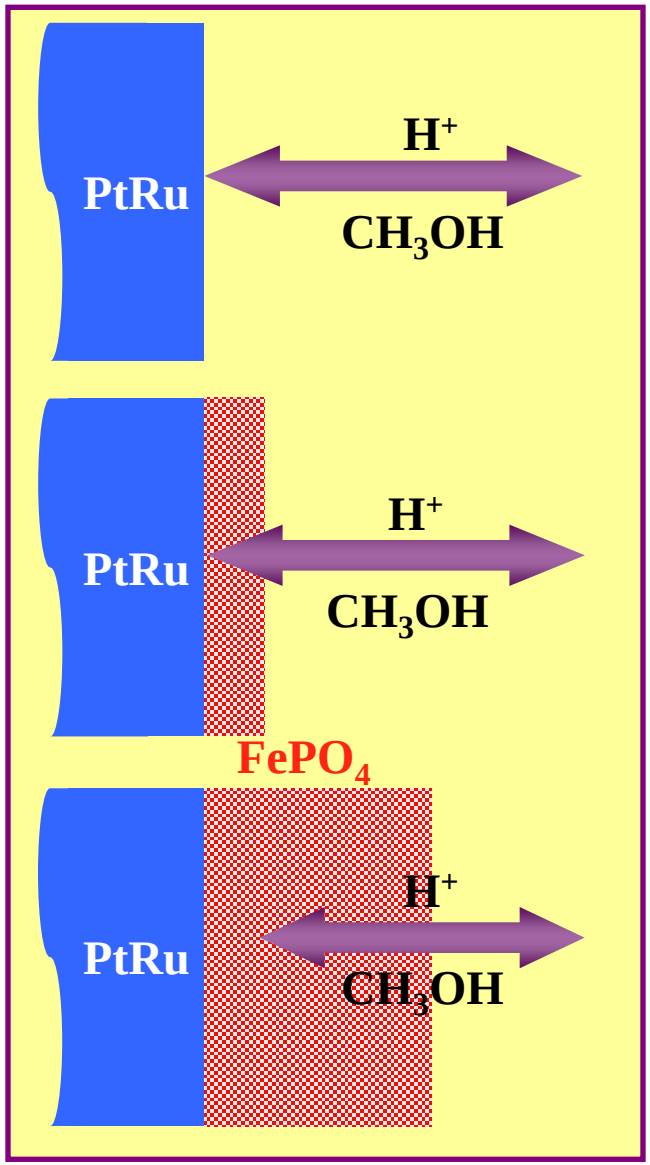

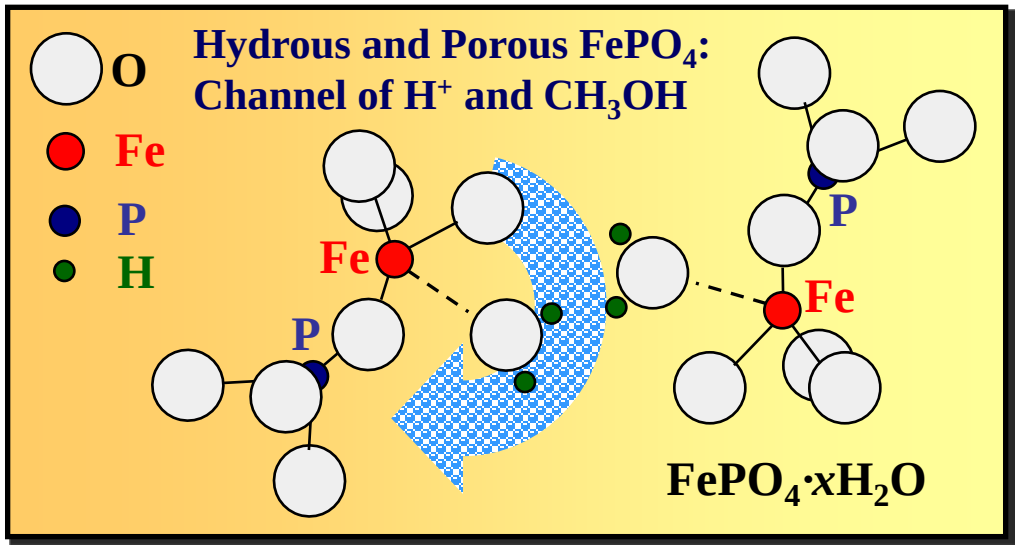

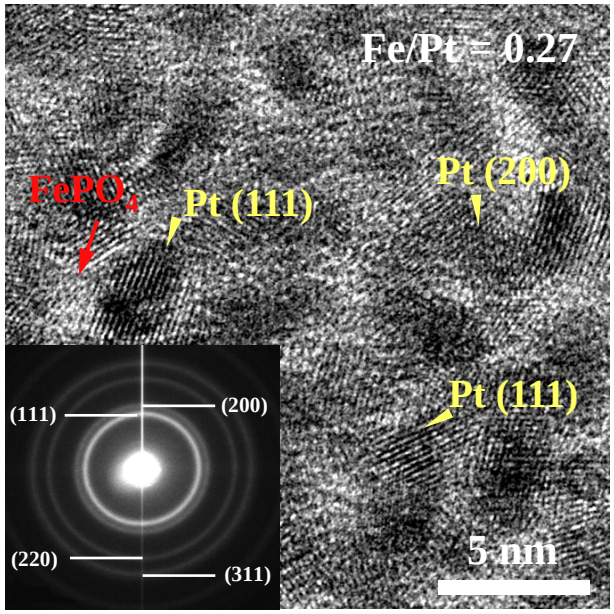

My Group
Electrochem. Solid-State Lett. (2006).

Determination of the Platinum and Ruthenium Surface Areas in Platinum−Ruthenium Electrocatalysts by Underpotential Deposition of Copper. 2. Effect of Surface Composition on Activity

Clare L. Green and Anthony Kucernak*

Department of Chemistry, Imperial College of Science Technology and Medicine, London SW7 2AY, U.K.

Received: April 1, 2002; In Final Form: July 30, 2002

Submonolayer amounts of Ru have been deposited on a polycrystalline Pt bead electrode from a solution containing 6.68×10^{-4} mol dm^{-3} $RuNO(NO_3)_3$ using an impinging jet apparatus. Deposition of Ru on a platinum surface almost completely covered with H_{ads} due to exchange of the adsorbed hydrogen with Ru^{3+} produces a surface coverage of 0.12 ± 0.02. The reduction of Ru occurs via two separate pathways: in one, metallic Ru is deposited on the surface; in the other, the complex is reduced to an intermediate oxidation state and remains soluble. The latter process, which occurs at potentials less than about 0.25 V has not been previously reported and may explain some of the discrepancies seen in the literature. For characterization of the resultant Pt(Ru) surface we compare the approach developed by Motoo and Watanabe (*J. Electroanal. Chem.* **1975**, *60*, 267−273)[1] and Frelink et al. (*Langmuir* **1996**, *12*, 3702)[2] with that utilizing copper upd. The latter approach is applicable for Ru coverage from 0 up to at least 0.80, whereas the former methods are only applicable up to a coverage of ca. 0.30. On addition of Ru to a clean Pt surface a small initial drop in total surface area is seen, but the area then remains quite constant with increasing Ru coverage. In comparison, the charge measured from stripping of a saturated CO layer adsorbed at 0.3 V(RHE) shows an increase with Ru coverage. The most active surface for the oxidation of an adsorbed CO layer as measured by the potential at which half of the CO has been oxidized is found to contain a Ru surface coverage of 0.2. In comparison, for the oxidation of methanol at 25 °C, it is found that there is a broad maximum in catalytic activity for Ru surface coverage in the range 0.25−0.5. The long term poisoning rate of the electrodes is highly dependent upon Ru coverage, showing a minimum over the range 0.4−0.6.

Motivation: Change of Voltammogram due to Ru Deposition on Pt

Cyclic voltammogram of Pt in Ru^{+}-dissolved electrolyte: Spontaneous Ru deposition on Pt

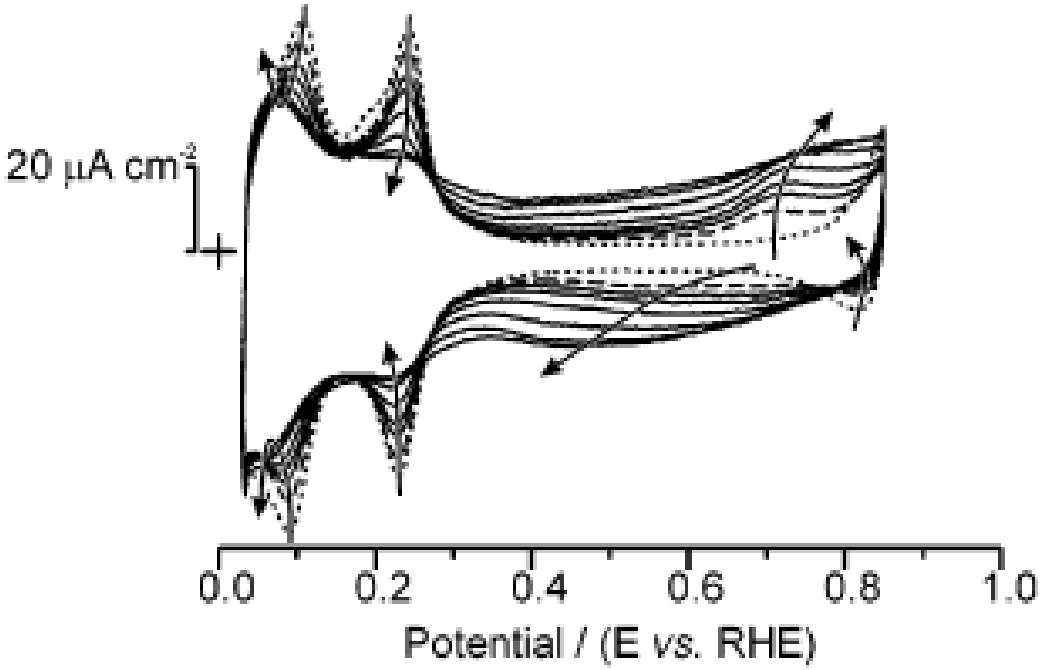

Kucernak's Group, Imperial College of Science Technology,
J. Phys. Chem. B (2002).

Ru Deposition on Pt Surface: The Loss of Pt Nature

$FePO_4$ Coating Layer for Blocking Ru Crossover

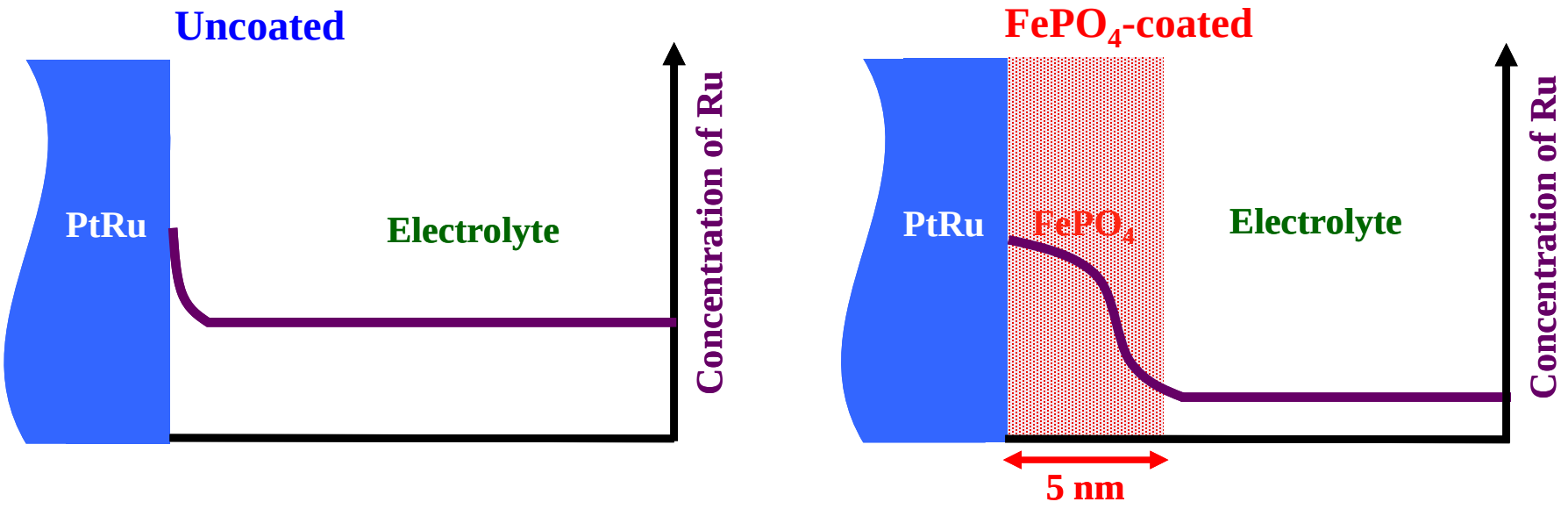

	Before 200 accelerated cycles	After 200 accelerated cycles		
	ESA (per 1 cm^2 sample)	*ESA* (per 1 cm^2 sample)	Ru dissolution into electrolyte	
			(per 1 cm^2 sample)	(normalized by *ESA*)
Uncoated	0.60 cm^2	1.06 cm^2	1.63 ± 0.39 ppb/cm^2	2.72 ± 0.65 ppb/cm^2
$FePO_4$-coated (5 nm)	1.05 cm^2	1.67 cm^2	1.97 ± 0.44 ppb/cm^2	1.88 ± 0.42 ppb/cm^2
$FePO_4$-coated (20 nm)	1.08 cm^2	1.61 cm^2	1.78 ± 0.44 ppb/cm^2	1.65 ± 0.41 ppb/cm^2

❖ **Considering exposed PtRu surface area, the dissolved Ru species were retained within $FePO_4$-coated layer.**

Oxygen-Reduction Activity of Modified Au Catalyst

Various $Au/AlPO_4$ nanocomposites were synthesized:
~10 nm gold crystallites were aggregated with the interposed $AlPO_4$.

The transfer of electron density from $AlPO_4$ to Au:
Controlling the Au catalytic activities with the modification of electronic structure.

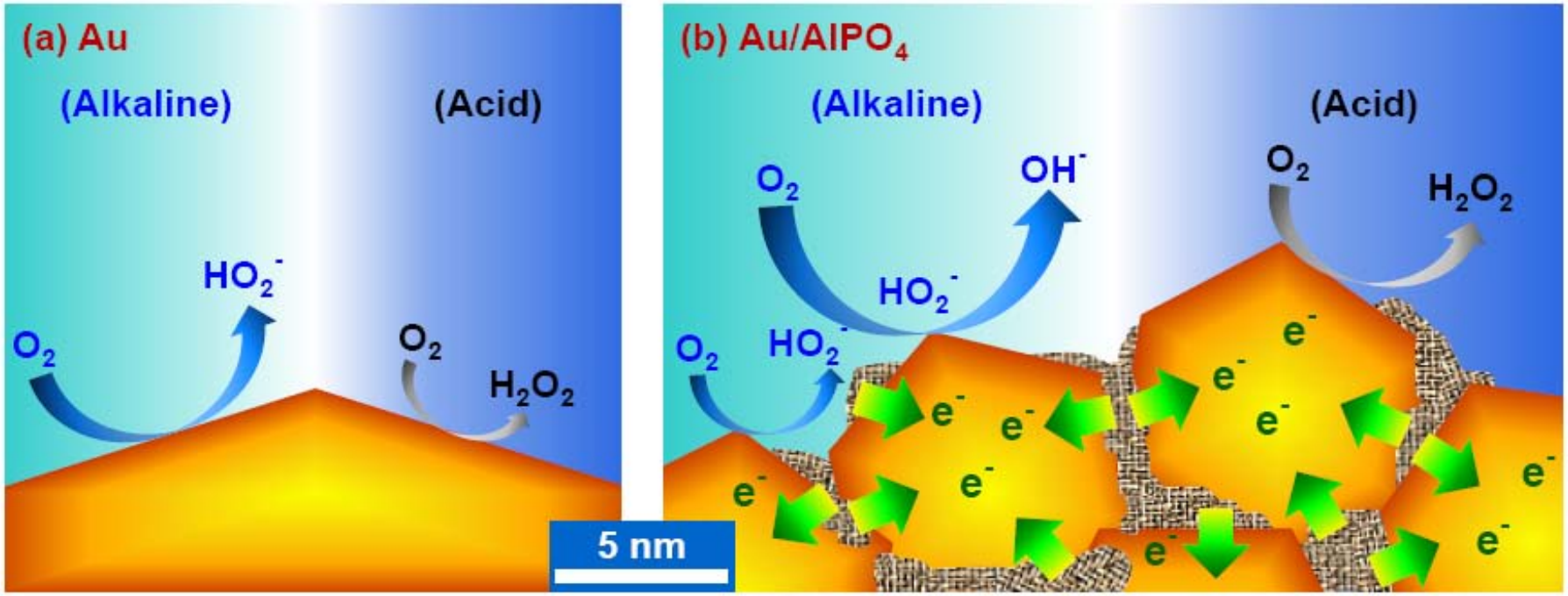

➢ Y. Park, B. Lee, C. Kim, J. Kim, S. Nam, Y. Oh, and **B. Park**, *J. Phys. Chem. C* (2010).

Conclusions

Nanoscale Interface Control

- Compositions?
- Nanostructures?
- Mechanisms?

http://bp.snu.ac.kr


THAT FUELCELL DOESN'T REALLY SOLVE THE PARKING-PROBLEM...
H2
http://www.imageproduction.nl